Performance Evaluation of Virgin and Recycled Aggregate Bases Stabilized with Geotextiles

By

Zexia Li

Submitted to the graduate degree program in Civil, Environmental, and Architectural Engineering and the Graduate Faculty of the University of Kansas in partial fulfillment of the requirements for the degree of Master of Science.

_____

Dr. Jie Han, Chairperson

_____

Dr. Jian Li

_____

Dr. Robert L. Parsons

Date Defended: 8/31/201

The Thesis Committee for Zexia Li certifies that this is the approved version of the following thesis:

Performance Evaluation of Virgin and Recycled Aggregate Bases Stabilized with Geotextiles

_____

Dr. Jie Han, Chairperson

Date Defended: 8/31/2018

Abstract

Virgin granular base (VGB) is currently the most widely-used base course material for roadway construction. As VGB in high demand, alternative materials, such as recycled concrete aggregate (RCA), have been increasingly used as a base material. Normally, a base material is placed directly on top of compacted subgrade soil in the field. When the subgrade is soft, it may not able to support the traffic or be intermixed with the base course subjected to loading. Geotextile can be placed in between the subgrade and the base course to minimize these effects. Serving as a separation function, the geotextile restrains particles from moving up and down. This research evaluated the performance of virgin granular aggregate and recycled concrete aggregate bases stabilized with geotextiles. Six large-scale cyclic plate loading tests were conducted on base courses placed on soft subgrade. Woven and non-woven geotextiles were used at the interface between base and subgrade to stabilize both VGB and RCA sections. The test results show that all the RCA base course sections outperformed the VGB base course sections in terms of their permanent deformation, bearing capacity, and stress distribution. Geotextile improved the performance of base courses in terms of their permanent deformation, bearing capacity, and stress distribution.

Acknowledgements

I would like to express my appreciation to my advisor, my mentor, Dr. Jie Han for providing me the amazing opportunity to conduct research on this project. He provided such a great platform for me to learn how to be a decent researcher, professional, and good person. This research was impossible without his guidance and encouragement. I also want to thank Dr. Robert L. Parsons for giving me the opportunity to work as his teaching assistant. It is an excellent experience for me to learn the most important and basic aspects of geotechnical engineering, which will benefit me greatly in my future career. I want to thank Dr. Jian Li for being in my graduate committee to advice and support my defense.

This research project was financially supported by Kansas Department of Transportation. This support is much appreciated.

When I was an undergraduate student at the University of Kansas, I was introduced to this research team by Dr. Jun Guo as an undergraduate research assistant. He continued to help me until today. This project would be much more difficult without his help. I also appreciate Dr. Fei Wang's unconditional help throughout my entire graduate school time. I would also thank Tanya Walkenbach for being the most amazing teammate I could ever ask for. We went through countless difficulties in this project. Without her dedication and encouragement, the completion of this thesis would be impossible.

I would like to thank all my friends in the KU geotechnical society who would always have my back.

Finally, I would like to express my appreciation to my parents for supporting me unconditionally since day one of my life. Words cannot describe the gratitude I have towards them. I would also like to thank my girlfriend for her support.

Table of Contents

Abstract ..... **ii**

Acknowledgements ..... **iii**

List of Figures ..... **vi**

List of Tables ..... **ix**

Chapter 1 INTRODUCTION **1**

1.1 Background 1

1.2 Problem Statement 3

1.3 Research Objective 5

1.4 Organization 5

Chapter 2 LITERATURE REVIEW **6**

2.1 Introduction 6

2.2 Geosynthetics 6

2.3 Base Material 9

2.4 Design Methods 14

2.5 Previous Relevant Studies 17

2.6 Summary 19

Chapter 3 Materials and Test Sections **21**

3.1 Introduction 21

3.2 Material Properties 21

3.3 Test Equipment and Setup 28

Chapter 4 Results and Analysis **42**

4.1 Introduction 42

4.2 Total Deformation versus Number of Loading Cycles.....42

4.2 Permanent Deformation Result Analysis.....46

4.4 Subgrade Pressure Analysis.....61

4.5 Comparison of Base Material Performance.....71

Chapter 5 Conclusions and Recommendations 73

5.1 Conclusions.....73

5.2 Recommendations for Future Studies.....74

References.....75

List of Figures

Figure 1.1 Common cross section of rigid pavement 2

Figure 1.2 U. S apparent consumption of raw material 2

Figure 1.3 Material estimated to be used in the national highway system in 2006 (Unit: million metric ton) 3

Figure 2.1 Inter-mixing effect 7

Figure 2.2 Lateral restrain effect 8

Figure 2.3 Tensioned membrane effect 9

Figure 3.1 Gradation of subgrade mix 21

Figure 3.2 CBR vs. moisture content of the subgrade 22

Figure 3.3 Undrain shear strength VS. CBR 23

Figure 3.4 Gradation curves of VGB and RCA 24

Figure 3.5 Standard Proctor compaction curve of virgin granular base 25

Figure 3.6 RCA standard Proctor curve 25

Figure 3.7 Woven geotextile 27

Figure 3.8 Woven geotextile 28

Figure 3.9 Large geotechnical test box 30

Figure 3.10 Test section setup 31

Figure 3.11 Earth pressure cell 31

Figure 3.12 Data loggers 32

Figure 3.13 Laptop monitoring program 32

Figure 3.14 CBR profiles for the control VGB test section 35

Figure 3.15 CBR profiles for the non-woven geotextile-stabilized VGB test section 36

Figure 3.16 CBR profiles for the woven geotextile-stabilized VGB test section 36

Figure 3.17 CBR profiles for the control RCA test section 37

Figure 3.18 CBR profiles for the non-woven geotextile-stabilized RCA test section 37

Figure 3.19 CBR profiles for the woven geotextile-stabilized RCA test section 38

Figure 4.1. Displacement vs. number of cycles for all test sections 44

Figure 4.2. Displacement VS. number of cycles for all VGB sections 44

Figure 4.3. Displacement VS. number of cycles for all RCA sections 45

Figure 4.4 VGB test section showing punching of the loading plate 45

Figure 4.5 Top view of the VGB test section punched by the loading plate 46

Figure 4.6 Permanent deformation vs. the number of cycles for VGB sections in Stage 6 under the applied pressure of 103 kPa 47

Figure 4.7. Permanent deformation vs. the number of cycles for VGB sections in Stage 7 under the applied pressure of 138 kPa 48

Figure 4.8 Permanent deformation vs. the number of cycles for VGB sections in Stage 8 under the applied pressure of 207 kPa 49

Figure 4.9 Permanent deformation vs. the number of cycles for VGB sections in Stage 9 under the applied pressure of 276 kPa 50

Figure 4.10. Permanent deformation vs. the number of cycles for VGB sections in Stage 10 under the applied pressure of 345 kPa 51

Figure 4.11 Permanent deformation vs. the number of cycles for RCA sections in Stage 6 under the applied pressure of 103 kPa 53

Figure 4.12 Permanent deformation vs. the number of cycles for RCA sections in Stage 7 under the applied pressure of 138 kPa 54

Figure 4.13 Permanent deformation vs. the number of cycles for RCA sections in Stage 8 under the applied pressure of 207 kPa 55

Figure 4.14 Permanent deformation vs. the number of cycles for RCA sections in Stage 9 under the applied pressure of 276 kPa 56

Figure 4.15 Permanent deformation vs. the number of cycles for RCA sections in Stage

10 under the applied pressure of 345 kPa 57

Figure 4.16 Permanent deformation vs. the number of cycles for RCA sections in Stage 11 under the applied pressure of 414 kPa 58

Figure 4.17 Applied pressure vs. Elastic deformation for all VGB sections 59

Figure 4.18 Applied pressure vs. Elastic deformation for all RCA sections 60

Figure 4.19 Measured subgrade pressures at 0R, 1R, and 2R from the center at the end of Stage 6 loading 63

Figure 4.20 Measured subgrade pressures at 0R, 1R, and 2R from the center at the end of Stage 7 loading 63

Figure 4.21 Measured subgrade pressures at 0R, 1R, and 2R from the center at the end of Stage 8 loading 65

Figure 4.22 Measured subgrade pressures at 0R, 1R, and 2R from the center at the end of Stage 9 loading 65

Figure 4.23 Measured subgrade pressures at 0R, 1R, and 2R from the center at the end of Stage 10 loading 67

Figure 4.24 Measured subgrade pressures at 0R, 1R, and 2R from the center at the end of Stage 11 loading 67

Figure 4.25 Permanent deformations in the VGB and RCA control sections 72

List of Tables

Table 2.1 Gradation requirements for aggregate materials 10

Table 2.2 Granular base material gradation requirement 10

Table 2.3 Recycled concrete material properties and suggested test methods 12

Table 3.1 Loading sequence 33

Table 3.2a Average CBR and standard deviation for subgrade and base course in all VGB sections 39

Table 3.2b Average CBR and standard deviation for subgrade and base course in all RCA sections 39

Table 3.3 Subgrade LWD test results 40

Table 3.4 Base course LWD test results 40

Table 3.5 Sand cone test results for base courses in the test sections 41

Table 4.1 Total and Stage 6 permanent deformations for VGB sections 48

Table 4.2 Total and Stage 7 permanent deformations for VGB sections 49

Table 4.3 Total and Stage 8 permanent deformations for VGB sections 50

Table 4.4 Total and Stage 9 permanent deformations for VGB sections 51

Table 4.5 Total and Stage 10 permanent deformations for VGB sections 52

Table 4.6 Final permanent deformations and total loading cycles for all VGB sections 52

Table 4.7 Total and Stage 6 permanent deformations for RCA sections 53

Table 4.8 Total and Stage 7 permanent deformations for RCA sections 54

Table 4.9 Total and Stage 8 permanent deformations for RCA sections 55

Table 4.10 Total and Stage 9 permanent deformations for RCA sections 56

Table 4.11 Total and Stage 10 permanent deformations for RCA sections 57

Table 4.12 Total and Stage 11 permanent deformations for RCA sections 58

Table 4.13 Elastic deformations for all VGB test sections 60

Table 4.14 Elastic deformations for all RCA test sections 61

Table 4.15 Measured subgrade pressures in all RCA sections at 0R, 1R, and 2R at the end of stage loading 69

Table 4.16 Measured subgrade pressures in all VGB sections at 0R, 1R , and 2R at the end of stage loading 70

Chapter 1 INTRODUCTION

1.1 Background

Figure 1-1 shows the typical cross section of a concrete pavement. Concrete pavement is one of two commonly-used pavement types. Concrete pavement can be placed directly on top of natural soil. As the traffic volume increases, problems, such as pumping of the fine particles, frost heave, and soil expansion, may develop (Hein et al. 2016). Placing a layer of granular material under the pavement will effectively eliminate the above problems. This granular layer is called base course. Since granular material can have better drainage, higher modulus, and better stress distribution, it enhances the performance of the pavement and prolong the design life of the pavement. As the traffic volume keeps increasing, thicker and thicker granular bases have been designed and built under pavements. This dramatically increases the demand for granular material.

Virgin granular material is the most common base coarse material to be placed on top of natural subgrade. Figure 1-2 shows that nature aggregates are the most dominant building material consumed in the United States, i.e., more than 2,000 million metric tons per year since 1990 (Sullivan 2006). This number has kept growing. By the beginning of 21st century, more than 3000 million metric tons of nature aggregates were consumed in the United States. Figure 1-3 shows the estimated material consumption in highway construction in 2006 including 1500 million metric tons of nature aggregate. Both figures show that nature aggregates are in very high demand especially for pavement applications. Recycled material was less commonly used than natural aggregate as shown in Figures 1.2 and 1.3. In 1990, only less than 500 million metric tons of recycled material were consumed. The amount of recycled material consumed has not changed much throughout the years.

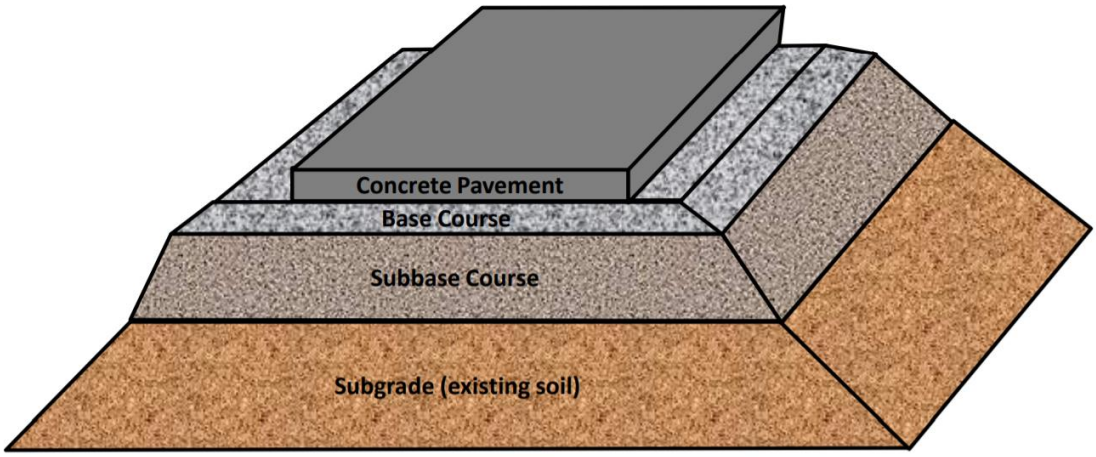

Figure 1.1 Common cross section of rigid pavement (Hein et al. 2016)

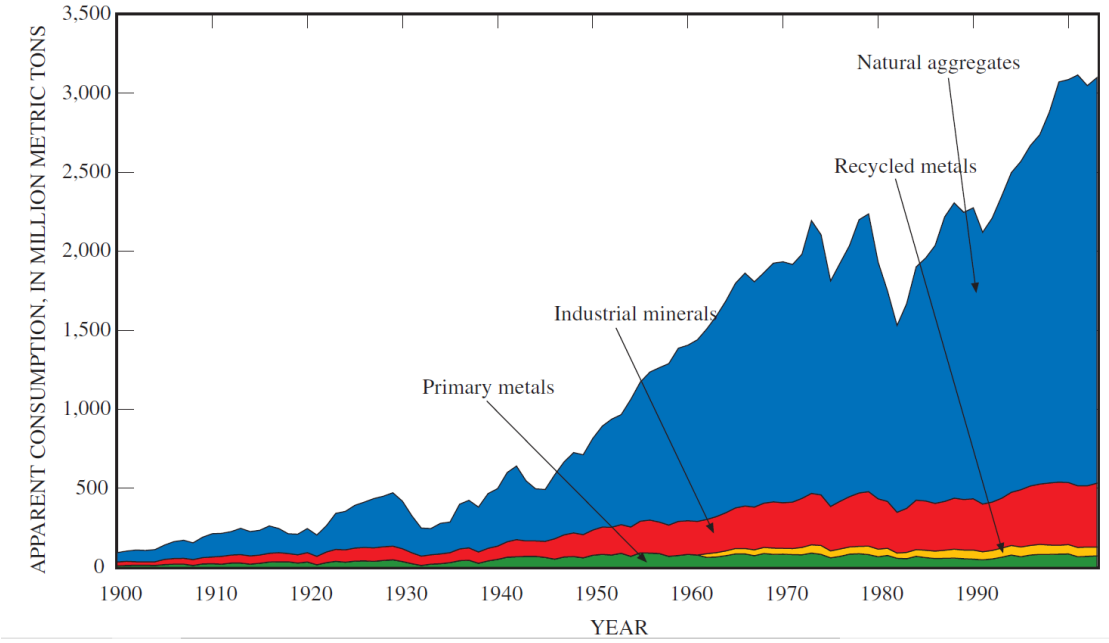

Figure 1.2 U.S apparent consumption of raw material (Sullivan 2006)

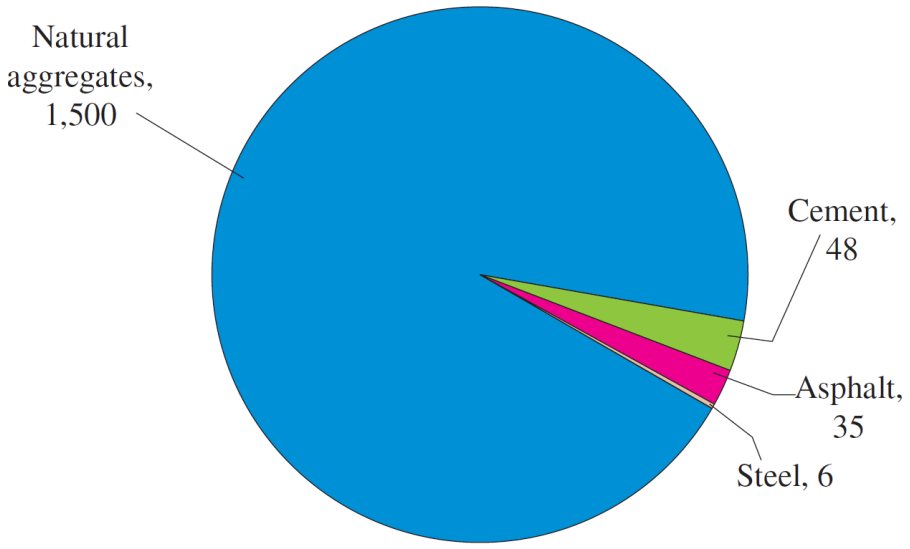

Figure 1.3 Material estimated to be used in the national highway system in 2006 (Unit: million metric ton) (Sullivan 2006)

Geosynthetic materials have been widely used in modern construction. Geosynthetic reinforcement is considered as a method of ground improvement. Common geosynthetic materials include geogrid, geotextile, geomembrane, geonet, geopipe, geosynthetic clay liner, geofoam, geocell, and geocomposite, which are used in all sorts of projects including slopes, embankments, earth retaining systems, foundations, landfills, railroads, and pavements. Geogrid, geotextile, and geocell are common geosynthetic materials used for pavement applications. The cost benefit of these products is greatly recognized in the industry. The functions that the geosynthetic materials provide are separation, reinforcement, stabilization, filtration, drainage, and containment.

1.2 Problem Statement

In such high demand for virgin aggregates, low-cost alternative base material, such as recycled concrete pavement (RCP), has been considered and used as an alternative base material throughout America and Europe. The American Association of State Highway and Transportation Officials (AASHTO) considered RCP as one type of base material

(AASHTO, 2015). More studies about the characteristics and properties of both materials will be further discussed in the next chapter of this thesis.

Although base course will prolong the life of the pavement, problems, such as pumping, reflection cracking, fine migration, layer intermixing, and other problems, still exist and these problems affect the structural integrity of the pavement. One of the solutions for most of these problems is to add geosynthetic materials. Geosynthetic materials have been widely used in flexible pavements and unpaved roadways. There are plenty of design methods for both geosynthetic-stabilized flexible pavements and geosynthetic-stabilized unpaved roads. Giroud and Han developed a design method for geogrid-stabilized unpaved roads (Giroud and Han 2004). This is one of the most commonly-used unpaved road design methods. AASHTO developed design methods for both rigid and flexible pavements. The flexible pavement design method (AASHTO 1993) was modified for geosynthetic-stabilized flexible pavement design by the geosynthetic industry. However, there is not sufficient study and research done to show the benefit of geosynthetic-stabilized granular base or RCP base for rigid pavements.

In this research, six large box tests were done to examine geosynthetic-stabilized granular base and geosynthetic-stabilized RCP base on soft subgrade. Woven geotextile or non-woven geotextile was placed at the interface of base course and soft subgrade to separate the base course from the subgrade. The geotextile is expected to prevent the material from intermixing between these two layers. The intermixing effect reduces the effective thickness of the base course and the modulus of the base course. When excessive deformation occurs, the geosynthetic layer can provide a tensioned membrane effect, which will be further explained in the literature review chapter.

1.3 Research Objective

The objective of this research was to investigate the performance of virgin granular base and recycled concrete pavement with and without a geosynthetic layer on soft subgrade. As mentioned before, two types of geosynthetic material, woven and nonwoven geotextile, were used. This study aimed at providing evidence, theoretical basis, and test data for future development of design method for geosynthetic-stabilized recycled (reclaimed) rigid pavements.

1.4 Organization

This thesis contains five chapters. The first chapter provides an overview of this study. The second chapter will review the literature on base materials, geosynthetics, pavement design and parameters, and previous studies on similar topics. The third chapter provides the material properties, the test setup, and the results of dynamic cone penetrometer and light-weight deflectmeter. The forth chapter discusses and analyzes the test results, including permanent deformation, elastic deformation, and subgrade pressure. The fifth chapter provides the conclusions and future study recommendations.

Chapter 2 LITERATURE REVIEW

2.1 Introduction

This chapter provides a literature review of the properties and functions of geosynthetics, aggregate base material, recycled concrete pavement, and pavement design methods.

2.2 Geosynthetics

Geosynthetics have different products. The commonly-used geosynthetics for roads are non-woven geotextile, woven geotextile, geogrid, and geocell. Even though this study was focused on non-woven geotextile and woven geotextile, the review of geogrid is also provided below because they are related. These geosynthetic products serve different functions. Webster (1993) summarized four functions of the geogrids in stabilized flexible pavements: separation, interlocking effect with aggregate base, subgrade confinement, and tensioned membrane effect. In his study, the geogrid-stabilized sections showed significant improvement in terms of rut depth vs. number of passes. His results also showed that placement of a geogrid at the bottom of a base layer would provide more improvement than that in the middle of the base layer (Webster 1993).

Maxwell et al. (2005) summarized three benefits provided by geosynthetics in road sections. They are: separation, lateral restraint, and tensioned membrane effect. Figure 2.1 shows the separation function by the placed geosynthetic. When roadways are subjected to high stresses and/or freeze thaw cycles, the aggregate in the base will sink into the subgrade. At the same time, the fines in the subgrade will be pumped into the base layer; therefore, inter-mixing of aggregate and subgrade happens. As a result, the base layer becomes thinner and weaker (Maxwell et al. 2005).

Kermani et al. (2018) conducted a series of labotory tests and summarized that migration of fines was significantly reduced by geotextile after high cycles of traffic loading. The amount of the migration of fines was related to the number of cycles applied. Pavement rut depth was reduced by 30% when the geotextile was placed at the interface of subgrade and subbase. By reducing the fine migration, the deformation of the subgrade was reduced. According to the piezometer reading, the migration of fines was triggered by the pore water pressure induced by dynamic traffic loading. Because of the placement of the geotextile separation layer, the pore water pressure was reduced (Kermani et al. 2018).

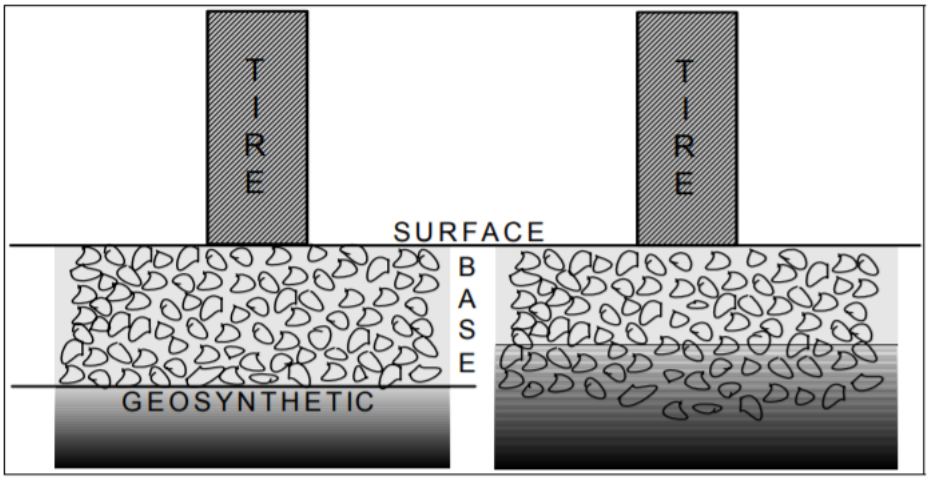

Figure 2.1 Inter-mixing effect (Maxwell et al. 2005)

Lateral restraint effect consists of four mechanisms as shown in Figure 2.2.

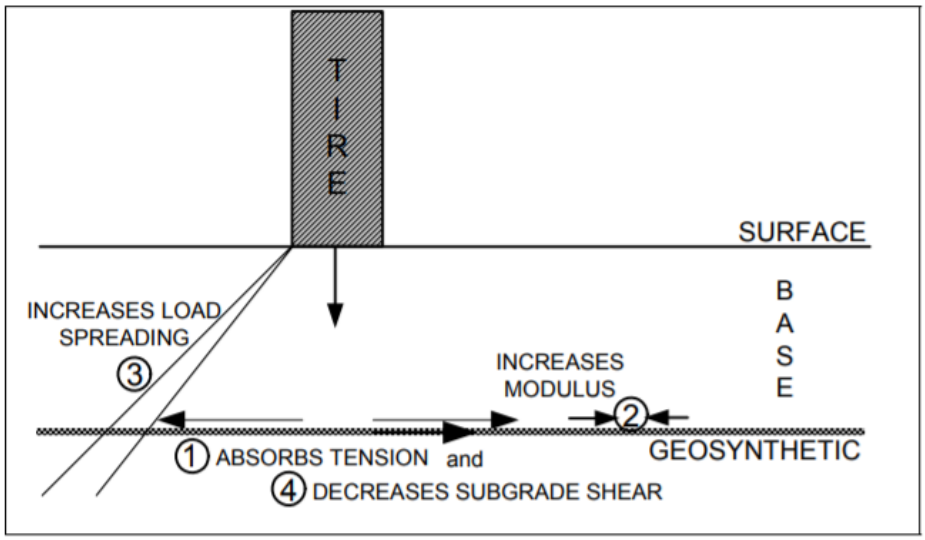

Figure 2.2 Lateral Restraint Effect (Maxwell et al. 2005)

(1) The shear force-induced by the traffic load at the bottom of the base layer causes the granular material to move downwards and outwards. The geosynthetic layer absorbs the shear stress to reduce the lateral deformation in the granular layer.

(2) The lateral resistance from the geosynthetic increases the confining stress in the lower portion of the base layer thus resulting in higher modulus of the base layer.

(3) The increase of the modulus increases the stress distribution angle from the base layer to the subgrade.

(4) The shear stress absorbed by the geosynthetic decreases the stress transfer on the subgrade.

Figure 2.3 shows the tensioned membrane effect. When large vertical deformation happens, the geosynthetic at the interface is stretched and tensioned (Giroud and Noiray 1981). The reason that this effect requires a large deformation to initiate is because only the vertical component of the tension in the geosynthetic can carry the vertical load and a large angle (i.e., large deformation) is required to have a large vertical tension

component.

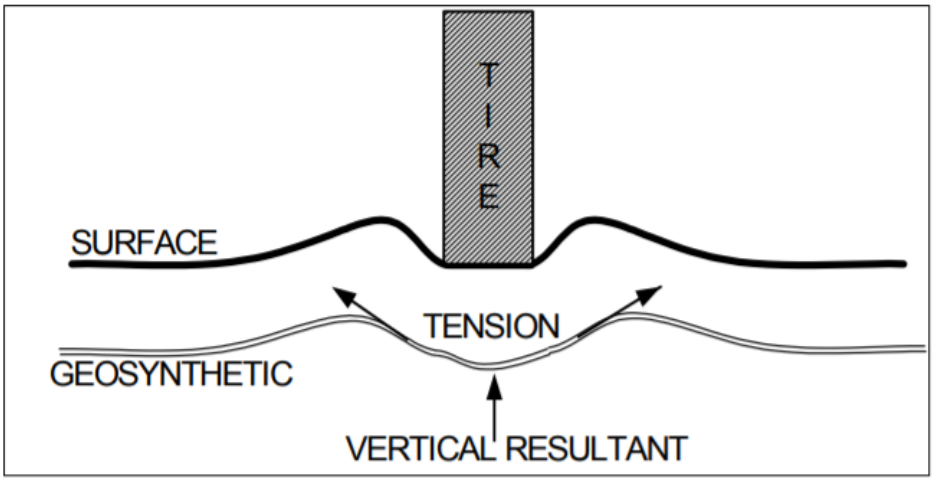

Figure 2.3 Tensioned membrane effect (Maxwell et al. 2005)

2.3 Base Material

2.3.1 Virgin Granular Base (VGB)

AASHTO (2011) stated that the gradation shown in Table 2.1 should be a reference gradation for base material. This table is developed for both asphalt and concrete pavements. Hein et al. (2016) stated that gradations B, D, E, and F should be adjusted since there are more than 15% passing No. 200 sieve. Hein et al. (2016) also stated that the maximum particle size of the base material should be less than 1/3 of the base thickness. The plasticity index should be equal or less than 6 and the liquid limit should be equal or less than 25. L.A. abrasion resistance should be 50% or less and the permeability should be less than 10^7 m/day (AASHTO 2011; Hein et al. 2016).

Table 2.1 Gradation requirements for aggregate materials (AASHTO. 2011)

Sieve Size	Percent Passing					
mm	Gradation A	Gradation B	Gradation C	Gradation D	Gradation E	Gradation F
50.8	100	100	-	-	-	-
25.4	-	75-95	100	100	100	100
19	30-65	40-75	50-85	60-100	-	-
4.76	25-55	30-60	35-65	55-85	55-100	70-100
2	15-40	20-45	25-50	40-70	40-100	55-100
0.42	8-20	15-30	15-30	25-45	20-50	30-70
0.074	2-8	5-20	5-15	5-20	6-20	8-25

Kansas Department of Transportation has the following requirements for granular bases used for concrete pavements (KDOT, 2018). The granular base should be a uniform mix of sand, gravel, crushed stone, and/or a suitable binder soil if any. The base material must have a minimum soundness of 0.85, maximum wear of 50% and maximum absorption of 4%. The material size distribution requirement is shown in Table 2.2.

Table 2.2 Granular base material gradation requirement (KDOT, 2018)

Sieve size	1 ½”	¾”	No. 4	No. 8	No. 40	No. 200
Percent Retained	0	0-15	10-65	25-70	50-90	85-95

The maximum liquid limit of the granular base is 25. The plasticity index of the mix containing more than 50% crushed limestone should be between 1 to 8, and that for all other aggregate combinations should range between 3 to 8 (KDOT, 2018).

2.3.2 Recycled Concrete Aggregate (RCA)

Since granular base is in high demand for construction, RCA has been considered as an alternative material for base coarse and sub-base layers in pavement construction. In addition, the use of recycled concrete will reduce the demand for virgin aggregate material and help reduce the environmental impact on the earth. This will also reduce solid waste. It will be more economic if RCA can be produced on or near project sites, so the hauling distance will be reduced significantly. This also means that the use of RCA will reduce the effect of hauling traffic on nearby roads. Recycling of a material is also an more economic option than waste deposal; therefore, the use of RCA will reduce the overall project cost (Gonzalez and Moo-Young 2004). Since RCA is 100 percent crushed, this material has high angularity. Mortar is the adhesion agent in concrete that attaches on aggregates to create rough surface. This characteristic makes RCA more porous and permeable. Table 2.3 shows the material properties of RCA and their test methods (Chesner 1998).

Silvakumar et al. (2004) found that recycled construction wastes, such as RCA, have high shear strength and can be utilized in geotechnical applications as an alternative material. However, their frictional resistance decreases with loading cycles (Sivakumar et al. 2004).

Table 2.3 Recycled concrete material properties test methods (Chesner 1998)

Property	Test Method	Reference
General Specifications	Graded Aggregate Material for Bases or Subbases for Highways or Airports	ASTM D2940
Gradation	Sizes of Aggregate for Road and Bridge Construction	ASTM D448/ AASHTO M43
	Sieve Analysis of Fine and Coarse Aggregate	ASTM C136/ AASHTO T27
Particle Shape	Flat and Elongated Particles in Coarse Aggregate	ASTM D4791
	Uncompacted Voids Content of Fine Aggregate (As Influenced by Particle Shape, Surface Texture, and Grading	AASHTO TP33
	Index of Aggregate Particle Shape and Texture	ASTM D3398
Base Stability	California Bearing Ratio	ASTM D1883/ AASHTO T193
	Moisture-Density Relations of Soils Using a 5.5 lb (2.5 kg) Rammer and a 12-in. (305 mm) Drop	ASTM D698/ AASHTO T99
	Moisture- Density Relations of Soils Using a 10-lb (4.54 kg) Rammer and an 18-in. (457 mm) Drop	AASHTO T180
Permeability	Permeability of Granular Soils (Constant Head)	ASTM D2434/ AASHTO T215
Plasticity	Determining the Plastic Limit and Plasticity Index of Soils	ASTM D4318/ AASHTO T90
	Plastic Fines in Graded Aggregates and Soils by Use of the Sand Equivalent Test	ASTM D2419/ AASHTO T176
Abrasion Resistance	Resistance to Degradation of Large-Size Coarse Aggregate by Abrasion and Impact in the Los Angeles Machine	ASTM C535
	Resistance to Degradation of Small-Size Coarse Aggregate by Abrasion and Impact in the Los Angeles Machine	ASTM C131/ AASHTO T96
Resilient Modulus	Resilient Modulus of Unbound Granular Base/Subbase Materials and Subgrade Soils - SHRP Protocol P46	AASHTO T274

Melbouci (2009) performed modified Proctor tests, California bearing ratio tests, hardness tests, and shear tests on RCA and found that the RCA did not perform as well as the virgin base material. The addition of a small amount of sand, cement, and brick element into the RCA (smaller than 0.125 mm) improved its mechanical resistance (Melbouci 2009).

Chidiroglou et al. (2008) conducted a series of investigations on RCA and concluded that the sieve analysis test should be conducted longer than 15 minutes in order to get the actual gradation result. The angularity of particles decreased with the particles size. Crushed concrete behaved similiarly if the composition was similar. The RCA material had similar water absorption if the gradation was similar (Chidiroglou et al. 2008).

Tam and Tam (2007) studied the physical characteristics of RCA and pointed out that a small percentage of cement was attached to the surface of large particles. The high porosity of the RCA material might cause larger deformation (Tam and Tam 2007).

Poon and Chan (2006) discovered that RCA was lighter than natural aggregate. After a four-day soaking period, the RCA had a negligible amount of swelling. The compaction curve of the RCA was flat, indicating water had less effect on its dry density (Poon and Chan 2006)

Arulrajah et al. (2012) conducted a study on different recycled materials including RCA. In their study, they found that the RCA had a much higher modulus and a much smaller permanent deformation than natural subbase materials. The RCA performed equally or even better than the virgin base aggregate in terms of pavement and geotechnical properties (Arulrajah et al. 2012).

Bennert et al. (2000) compared RCA, recycles asphalt, and densely-graded aggregate base coarses with similar gradation. The densely-graded aggregate had the highest

maximum dry density, 2098 kg/m^3, at 7% moisture content. The maximum dry density of the RCA was 1984 kg/m^3 at 7.5% moisture content. All specimens were tested under the same loading sequence. The results show that the RCA had the least amount of strain and the highest resillient modulus (Bennert et al. 2000).

2.4 Design Methods

This section will briefly review the design methods for unpaved roads, flexible pavements, and rigid pavements.

2.4.1 Stabilized Unpaved Road Design

The controlling failure mode for unpaved roads is bearing failure. Giroud and Noiray (1981) used bearing capacity factors N_c of 3.14 for unreinforced cases and 5.14 for reinforced cases in their design method. Giroud and Han (2004) developed a design method for georid-stabilized unpaved roads to calculate the required thickness of the base layer. This method considered not only N_c but also the improvement brought by geogrid reinforcement and the aperture stability modulus of geogrid as design inputs. This method was developed for geogrid-stabilized unpaved roads but it could also be recalibrated for design of unpaved roads with other geosynthetic materials (Giroud and Han 2004; Giroud and Han 2004).

2.4.2 Stabilized Flexible Pavement Design

One of the most common flexible pavement design methods in America is the 1993 AASHTO Pavement Design Guide. In this guide, all traffic loading is converted into 18-kip (80 kN) equivalent single axle load (ESAL). Design parameters include pavement layer thickness, layer modulus, drainage properties for all layers except the surface layer, design traffic volume converted into ESAL, reliability and error, initial serviceability index, and terminal serviceability index. To consider the benefits of the

stabilized base layer for flexible pavements using the 1993 AASHTO guide, two modified methods have been adopted in the practice. The traffic benefit ratio (TBR) method considers that the stabilized section takes more cycles to reach the designated rut depth than the non-stabilized section. With the increased cycles, the increase of the structural number is the benefit of geosynthetic reinforcement. As a result, the thickness of the base layer can be reduced. The layer coefficient ratio (LCR) method is based on the modulus improvement by stabilization with geosynthetic. The LCR value can be determined by large-scale laboratory testing. An empirical relationship was also developed between LCR and modulus improvement factor (Han 2015; Han 2015; Montanelli et al. 1997).

2.4.3 Rigid Pavement Design

Concrete pavement design method is also included in the 1993 AASHTO guide. Since the pavement surface is rigid, low stress is distributed to the base layer and subgrade. Currently, geosynthetic-stabilized base for rigid pavements is not common and there is no design method available.

Although there is no design guide for geosynthetic-stabilized rigid pavements, a few studies have been conducted to determine the mechanical properties of the geosynthetic-stabilized bases.

AASHTO (1993) suggested that the subgrade resilient modulus can be calculated by the following equation:

$$M_{r(sg)} = \frac{(1-\vartheta^2)\times P}{\pi r^2 \delta_{r,r'}} \qquad \text{Eq. 1}$$

where $M_{r(sg)}$ is the subgrade resilient modulus (kPa), and $\delta_{r,r'}$ is the resilient deflection (mm) at 2 or 3 times the radius of the plate (r) away from the center of the loading plate

when the plate is being unloaded during cyclic loading. ϑ is the Poisson ration and P is the cyclic load (N).

AASHTO also suggested that subgrade reaction modulus, k, which is an important design parameter in the AASHTO 1993 design guide for rigid pavements, can be calculated with the following equation:

$$k = \frac{M_r}{19.4} \qquad \text{Eq. 2}$$

where M_r is in psi and k is in pci.

The elastic solution can be used to calculate the in-situ composite M_r:

$$M_r = \frac{(1-\vartheta^2)\times\Delta\sigma_p r}{\delta_r} \times f \qquad \text{Eq. 3}$$

where M_r is the uncorrected in-situ composite resilient modulus, δ_r is the resilient deflection of the loading plate during unloading part of the cyclic loading, $\Delta\sigma_p$ is the deviator stress, which is the maximum stress minus the minimum contacting stress, r is the radius of the loading plate, and f is the shape factor (White and Vennapusa 2017).

Equation 3 can be used to calculate the in-situ composite modulus and Eq. 2 can convert the resilient modulus into the subgrade reaction modulus. Sun et al. (2015) found that in the geosynthetic-stabilized base, the resilient deformation could be larger than that in the control section. In this case, the calculated in-situ composite resilient modulus is falsely lower since the resilient deformation is higher. The benefit of geosynthetic cannot be shown with the result of this method. In other words, this equation is not valid for geosynthetic-stabilized bases over subgrade.

The lateral restraint effect is expected to improve the modulus of the base layer. The modulus ratio between geosynthetic-stabilized base and non-stabilized base is called

the modulus improvement factor (MIF) (Pokharel et al. 2010).

Sun et al. (2017) developed an equivalent modulus back-calculation method for granular bases. This method uses the permanent deformation to back-calculate the modulus ratio of the base to the subgrade. Since geosynthetic reduces the permanent deformation of the base due to the increased modulus, this method can capture the contribution of the geosynthetic. However, this method does have some requirements. First, this method requires an accurate measurement or assumption of the subgrade CBR. Second, this method requires a calibration of a non-stabilized section with known modulus as a control section. Both of these requirements can be easily satisfied by using in-situ testing methods, such as light-weight deflectometer and dynamic cone penetrometer. With the calibrated factor, a known subgrade CBR, and the permanent deformation under the loading plate, the stabilized base modulus can be calculated (Sun et al. 2017).

2.5 Previous Relevant Studies

Dong et al. (2010b) demonstrated that biaxial geogrid is not capable of providing uniform tensile strength in all directions. This research proved that biaxial geogrid is not the ideal stabilization material if the load comes from different directions, such as at the interface of base course and subgrade (Dong et al. 2010).

Qian et al. (2013) showed that the pressure applied on the subgrade under the base course increased as the loading cycles increased. This is due to the deterioration of the base course and reduction of the stress distribution angle. Triangular geogrid not only can reduce the maximum vertical pressure being distributed on the subgrade, it can also slow the reduction rate of the modulus ratio of base to subgrade as compared to the non-stabilized sections. The modulus ratio at failure in this study was approximately 5.0

(Qian et al. 2013).

Sun et al. (2015) conducted a series of large-scale cyclic plate loading tests on geogrid-stabilized base courses on 2% CBR subgrade at the University of Kansas. In this research, test sections were constructed and tested, which included three different base thicknesses. For each base thickness, one non-stabilized and two stabilized sections were constructed and tested. Their test results showed that the vertical stress at the top of the subgrade was reduced when the section was stabilized. There was more reduction on the vertical stress when a stiffer geogrid was used. The percent of vertical stress reduction was less when the thickness of the base was increased. The stabilization effect was more efficient at a higher load. The radial stress results showed that the geogrid confinement not only affected the bottom of the base but also the top of the subgrade. Surface deformation was mainly caused by the deformation of the subgrade. The resilient deformation of the test section with a geosynthetic was larger since there was more lateral recovery at the end of each cycle. This research also discovered that the rate of deformation decreased as the number of cycles increased under low loads; however, the rate of deformation increased with the number of cycles under high loads. This result implies that under a high pressure, bearing failure occurred (Sun et al. 2015).

Geotextile can effectively increase the CBR and bearing capacity of the base. It would also improve the level of compaction of the low part of the base layer (Hufenus et al. 2006; Subaida et al. 2009).

Black and Holtz (1999) discorved that heat-bonded geotextile is more likely to clog as compared with needle-punched geotextile. In their observation, the geotextile imporved the performance of the pavement, which was built on a very poor condition soil. Aggregate is more likely to damage the geotextile than construction damage. When the

subgrade was consolidated, the geotextile would not provide much improvement (Black and Holtz 1999).

German has used nonwoven geotextiles as pavement interlayers since 1981. Water can be trapped in the interlayer and weaken the base over time. Placing a geotextile can effectively reduce the amount of water from entering the interlayer. This technique can preserve the life span of pavements. It has been considered as a direct replacement for placing hot mix asphalt at the interlayer. This method is inexpensive, easy to place, and the construction time is significantly shorter than other available methods (Garber and Rasmussen 2010).

2.6 Summary

This chapter reviewed the functions of geosynthetics, properties of granular base material and recycled concrete aggregate, pavement design methods, and previous relevant studies. Below is the summary of this literature review:

1. Geosynthetic materials have been researched for years and now use of geosynthetics is a very common practice. In pavement applications, the geosynthetic can (a) separate base course from subgrade and prevent their intermixing; (b) laterally restrain the base material to stabilize the base and increase the modulus of the base course; and (c) provide the tension at the interface to increase the bearing capacity when excess deformation occurs.
2. Virgin granular base is still the most common base and subbase material for roadway construction. Due to the high demand, an alternative material, recycled concrete aggregate (RCA), has been researched for years. RCA is cheaper, lighter, and easier to obtain. A plenty of recent studies showed that RCA performed better than traditional aggregates.

3. Geosynthetic-stabilized pavement design had been intergraded in most of the current design methods for unpaved roads and flexible pavements. Rigid pavement design method, however, has not yet included the benefit of geosynthetics. To develop a design method for stabilized bases for rigid pavements, an accurate estimation of mechanical properties of the base material, such as resilient modulus and subgrade reaction modulus, is needed.
4. The previous studies have investigated the performance of geosynthetic-stabilized pavements; however, there is very limited study done on geosynthetic-stabilized rigid pavements. The research described in this thesis may serve as the beginning of the research on this topic.

Chapter 3 Materials and Test Sections

3.1 Introduction

This chapter documents the subgrade, base course, and geosynthetic materials used in this study and the test sections with and without geosynthetic constructed and tested to evaluate their performance. The equipment, test sections, instrumentation, test preparation, loading procedure, and properties of subgrade and base course in each test section are also discussed in this chapter.

3.2 Material Properties

3.2.1 Subgrade

In this study, the subgrade material was used to mimic a natural soft subgrade condition. The subgrade was prepared by mixing 30% kaolin clay with 70% Kansas River sand by dry weight. Figure 3.1 shows the grain size distribution of the subgrade mix determined following ASTM D421 2007.

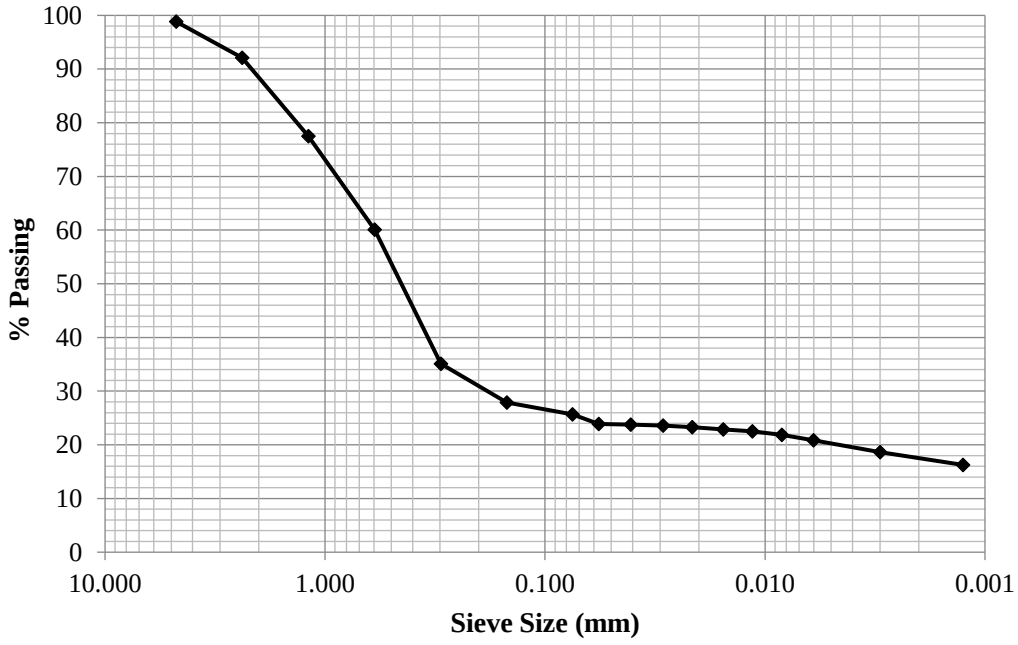

Figure 3.1 Gradation of subgrade mix

The plasticity index (PI) of the kaolin used in this mix was 24. The Kansas river sand used in this mix was a non-plastic (NP) material (ASTM D4318 2010). To select a desired California Bearing Ratio (CBR), a series of unsoaked CBR tests (ASTM D1883 2016) was conducted to find the relationship between the moisture content and the CBR value using standard Proctor compaction tests (ASTM D698 2012) as shown in Figure 3.2.

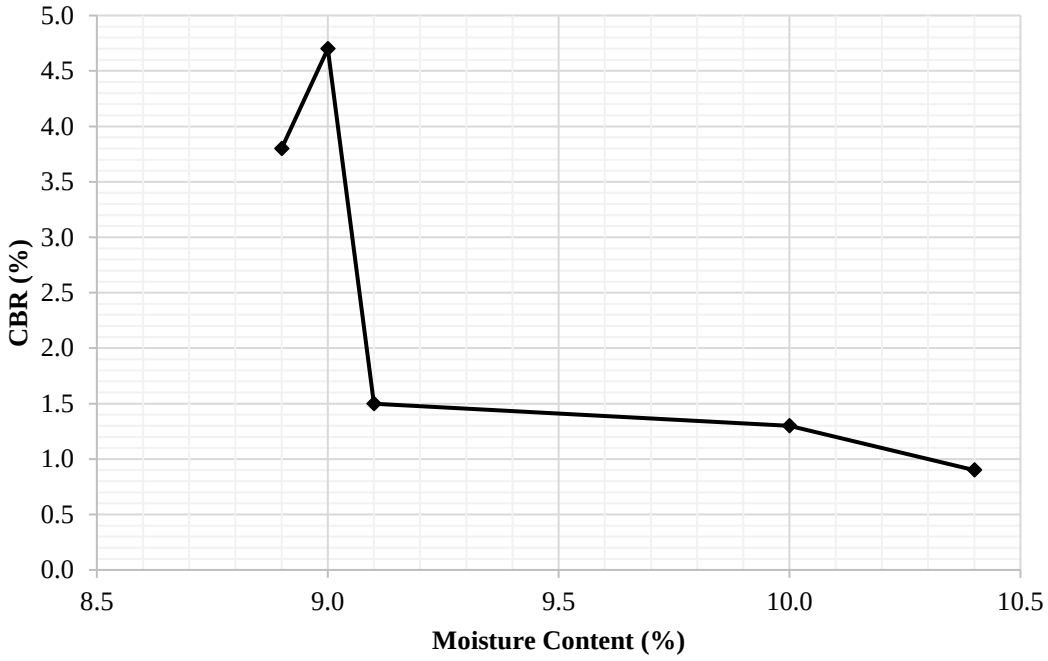

Figure 3.2 CBR vs. moisture content of the subgrade

Vane shear tests (ASTM D2573 2016) and unconfined compression (UC) tests (ASTM D2166 2016) were also conducted. Hand-held vane shear devices were used to determine the undrained shear strength of the subgrade. Hand-held vane shear device is a convenient way to check the undrain shear strength of the subgrade and useful to check the consistency of the subgrade in each test section. The unconfined compression tests were conducted to verify the strength obtained by the vane shear test. Figure 3.3 shows the relationship between CBR and undrained shear strength

determined by vane shear and unconfined compression tests.

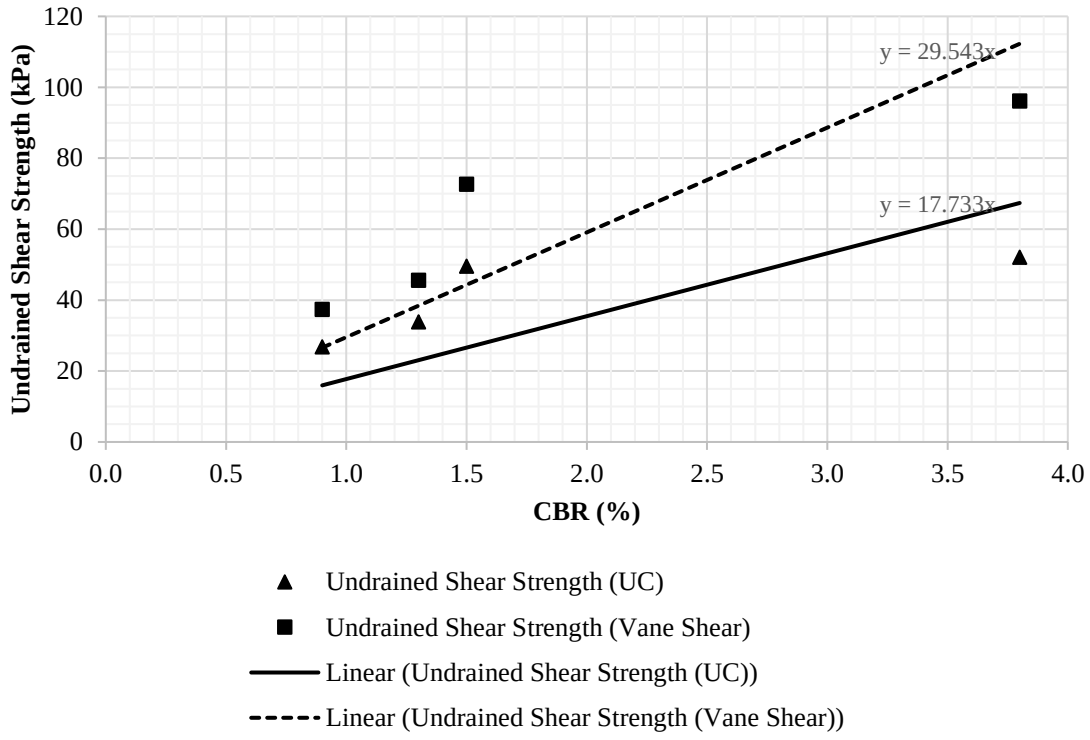

Figure 3.3 Undrain shear strength vs. CBR

In general, the shear strengths determined by the vane shear tests were higher than those by the unconfined compression tests. Their differences became larger at higher strengths.

3.2.2 Base Course Materials

Two types of base course materials were used in this study: virgin granular base (VGB) and recycled concrete aggregate (RCA). Table 2.2 shows the Kansas Department of Transportation (KDOT) requirements for base course materials used in Kansas. Figure 3.4 shows the gradation curves of VGB and RCA as compared with the required gradation limits for a granular base by KDOT. Both materials used in this study met the KDOT requirements. The coefficient of uniformity (C_u) was 33 for

the VGB and 365 for the RCA. The C_u values for both materials were larger than 6. The coefficients of curvature (C_c) waere 2.67 for VGB and 22.5 for RCA by using estimated $D_{10.}$ The VGB is a well graded material while the RCA is poorly graded.

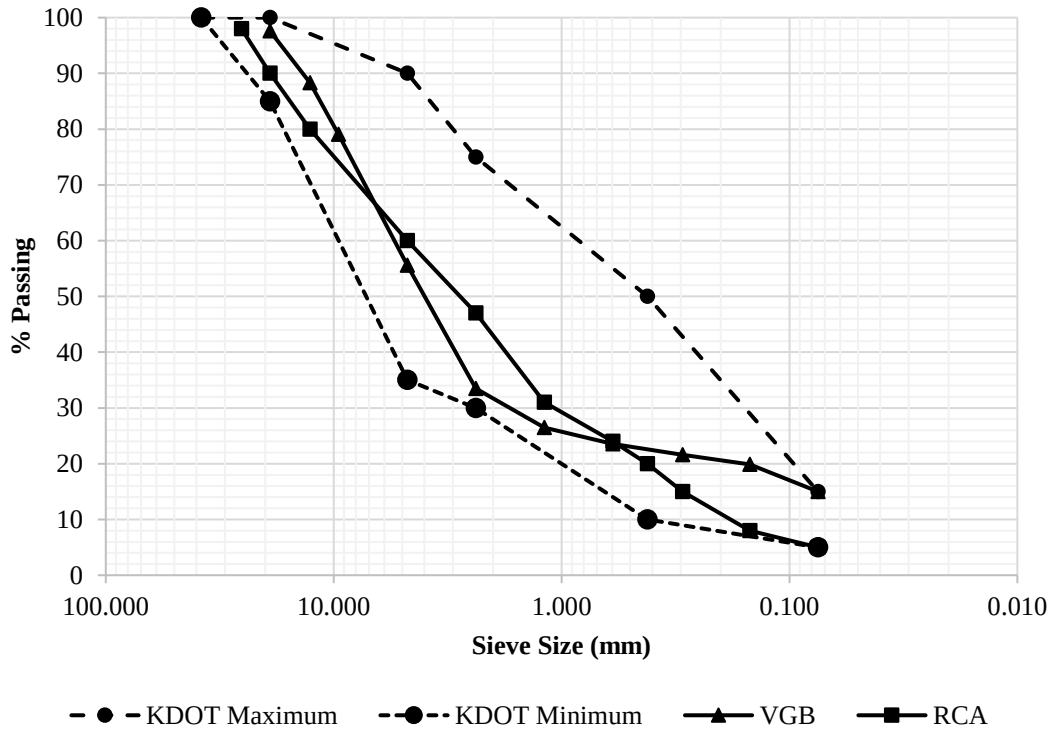

Figure 3.4 Gradation curves of VGB and RCA

Figure 3.5 shows the standard Proctor compaction curve for VGB. The optimum moisture content for VGB was 7.1% and its corresponding maximum dry unit weight was 21.2 kN/m^3. Figure 3.6 shows the standard Proctor compaction curve for RCA. The optimum moisture content for RCA was 14.1% and its corresponding maximum dry unit was 17.9 kN/m^3. The RCA had a lower maximum dry unit weight and a higher optimum moisture content than the VGB.

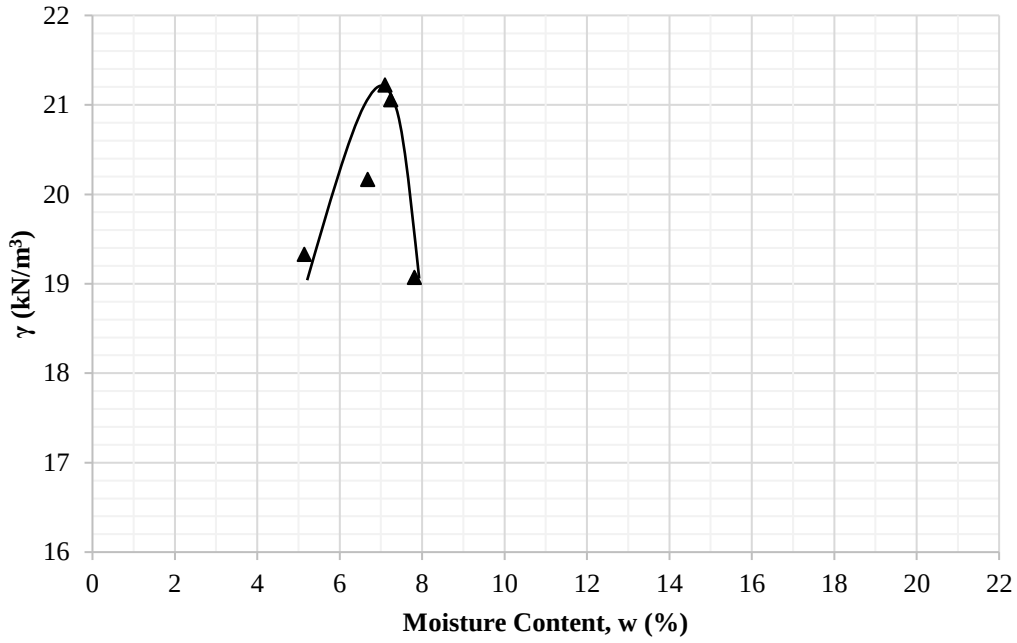

Figure 3.5 Standard Proctor compaction curve of virgin granular base

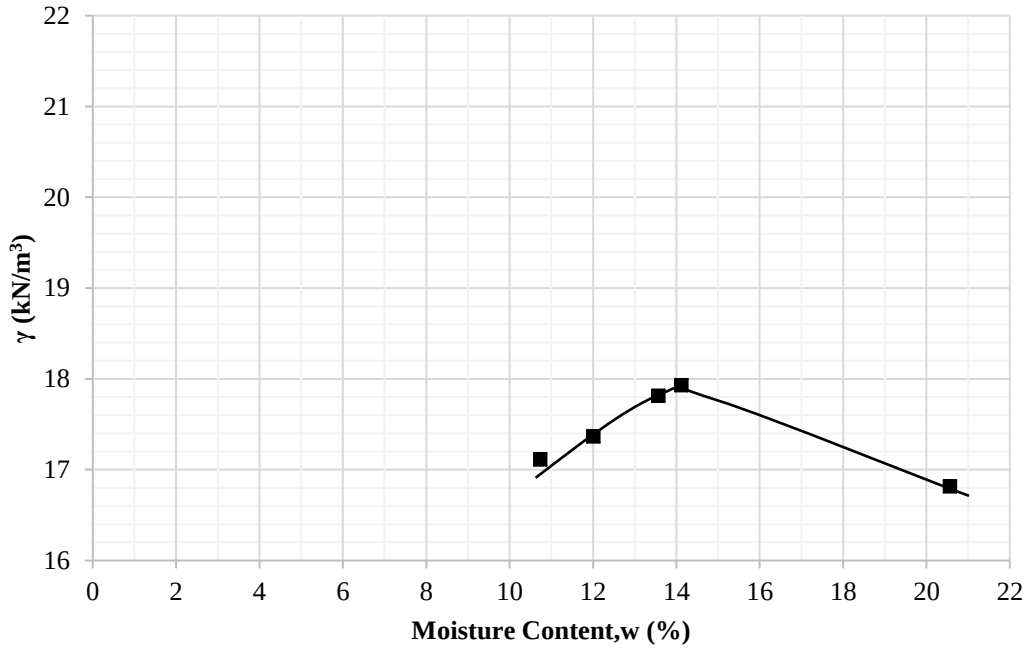

Figure 3.6 Standard Proctor compaction curve of RCA

3.2.3 Geosynthetic Material

Two commonly-used and pre-qualified geosynthetic products were selected and used in this study: (1) woven geotextile (WV), and (2) non-woven geotextile (NW). Based on the manufacturer's data sheet, the woven geotextile as shown in Figure 3.7 was a

polypropylene geotextile. This geotextile had a tensile strength of 14.0 kN/m in the machine direction, 19.3 kN/m in the cross-machine direction at 2% strain, and the ultimate strength of 70 kN/m in both directions. The apparent opening size (AOS), the flow rate, and the permittivity of this geotextile were 0.6 mm, 1222 L/min/m^2, and 0.4 sec^{-1}, respectively. The non-woven geotextile as shown in Figure 3.8 had a grab tensile strength of 712 N in both directions, a grab tensile elongation of 50%, a trapezoid tear strength of 267 N, and a CBR puncture strength of 1825 N. The AOS, the flow rate, and the permittivity of this geotextile were 0.212 mm, 4481 L/min/m^2, and 1.5 sec^{-1}, respectively. Based on the strength, the woven geotextile is stronger than the non-woven geotextile. The nonwoven geotextile had higher flow rate and permittivity than the woven geotextile. The non-woven geotextile had the smallest AOS. Since these geosynthetic products had quite different physical, mechanical, and hydraulic properties, direct comparison of their performance is difficult. The benefit of these geosynthetic products in this study should be evaluated based on their functions and mechanisms interacting with subgrade and base course.

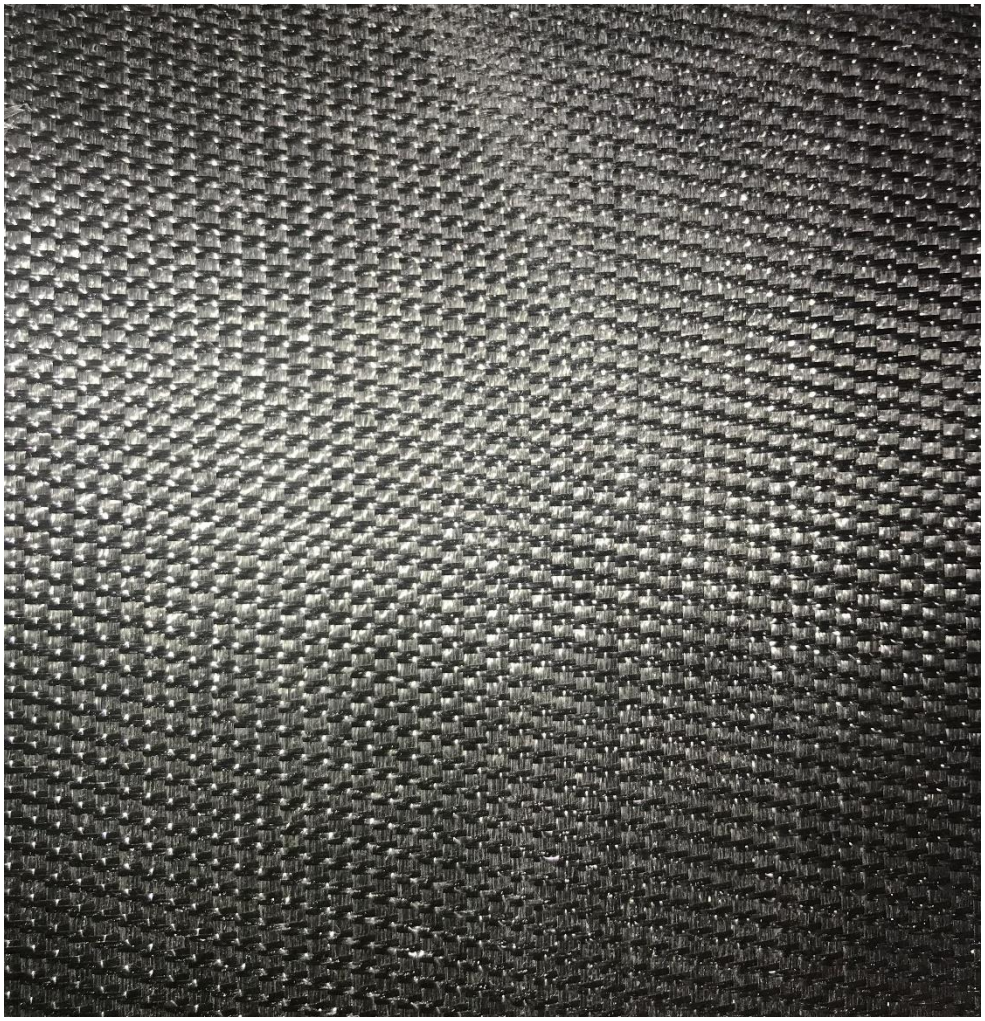

Figure 3.7 Woven geotextile

Figure 3.8 Non-woven geotextile

3.3 Test Equipment and Setup

3.3.1 Test Equipment and Test Sections

This study used a large geotechnical test box with dimensions of 2 m × 2.2 m × 2 m, as shown in Figure 3.9. Figure 3.10 shows a typical test section, which includes a subgrade, a geosynthetic sheet, and a base course. Six test sections were evaluated with two different base course materials and two geosynthetic products: (1) VGB without geosynthetic (Control VGB), (2) VGB/NW, (3) VGB/WV, (4) RCA without geosynthetic (Control RCA), (5) RCA/NW, and (6) RCA/WV. The base course thickness was approximately 250 mm in all test sections.

3.3.2 Instrumentation

Four earth pressure cells as shown in Figure 3.11 were used to measure the pressures at the interface between the base course and the subgrade induced by cyclic loading. These pressure cells were placed at 0, 0.15, 0.30, 0.45 m away from the center of the loading plate as illustrated in Figure 3.10.

All pressure cells were connected to a data logger as shown in Figure 3.12. The data loggers were connected to a laptop as shown in Figure 3.13, which recorded the pressure measurements at a frequency of 10 Hz (100 msec/log).

Figure 3.9 Large geotechnical test box

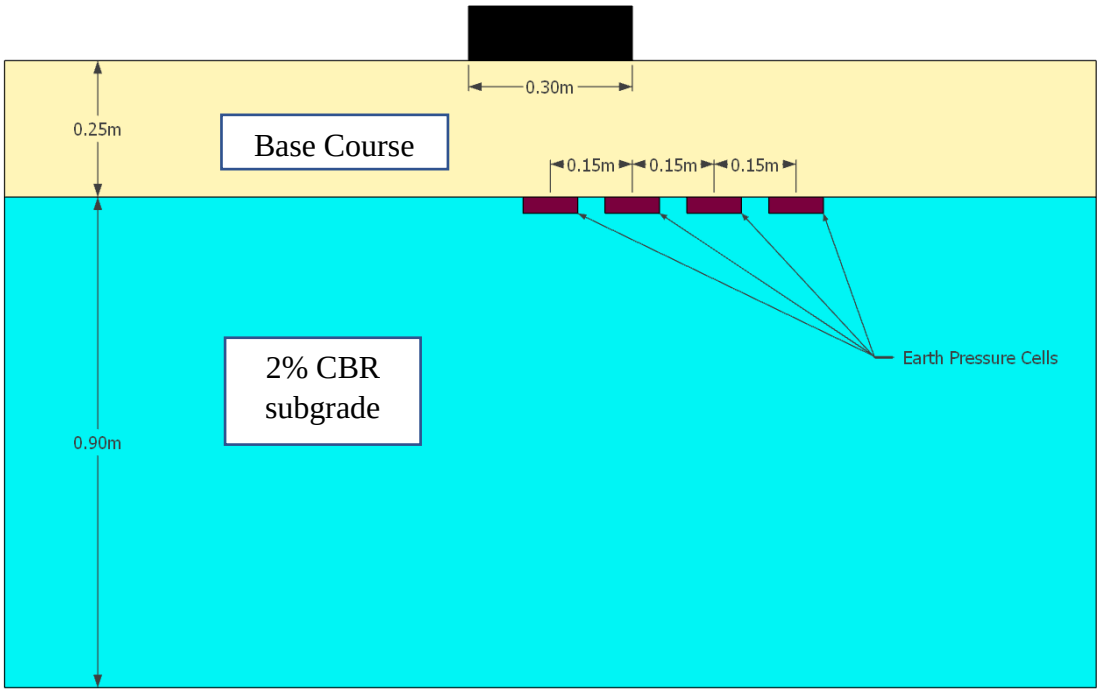

Figure 3.10 Test section setup

Figure 3.11 Earth pressure cell

Figure 3.12 Data loggers

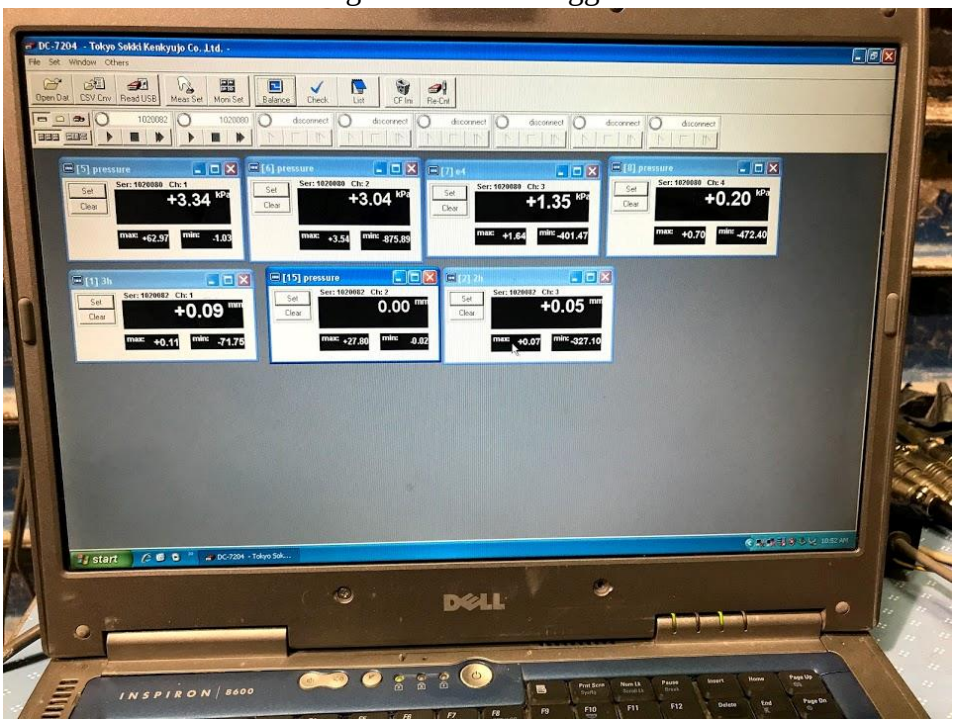

Figure 3.13 Laptop monitoring program

3.2.3 Loading Procedure

Static and cyclic plate loading tests were applied using the MTS hydraulic loading system to the test sections. All loads were applied on the test section with an actuator through a 300-mm diameter steel plate. Static loading was used as a preloading method. Preloading was used to seat the loading plate and ensure good contact between the loading plate and the base surface. 6.7 kN of force was applied on the loading plate. The static loading was finished once the deformation is stabilized.

Cyclic loading was applied on all test sections. Each load cycle included 0.3 second to reach to the maximum load, 0.3 second to hold the load,, 0.3 second to reduce the load to 0 kN, and then and 0.5 second to rest before next load cycle. . The cyclic loading sequence is summarized in Table 3.1.

Table 3.1 Loading sequence.

Loading Stage	**Applied Load (kN)**	**Simulated Tire Pressure (psi)**	**No. Cycles**
1	1.01	13.8	200
2	2.01	27.6	200
3	3.02	41.4	200
4	4.02	55.2	200
5	5.03	68.9	200
6	7.55	103.4	2,000
7	10.06	137.9	2,000
8	15.09	206.8	2,000
9	20.12	275.8	2,000
10	25.15	344.7	2,000
11	30.18	413.7	2,000

Each load cycle lasted 1.3 seconds and the test was terminated if one of the following two criteria was met:

1. The 13000 loading cycles were reached and
2. The maximum loading plate deformation was more than 40 mm (i.e., half of the failure criterion for unpaved roads, 75 mm).

3.2.4 Test Section Preparation

Each test section consisted of 0.91 m thick soft subgrade, 0.25 m thick base course, and a layer of geosynthetic material in between if needed. All subgrade was mixed with water to the desired moisture content, which was 9.8%. It corresponded to a CBR value of 2% under standard Proctor compaction energy. The subgrade soil was placed in six lifts and each lift was 0.15 m thick. After each lift was placed, it was levelled and compacted by a vibratory compactor to a desired density. The density of each lift was controlled by the weight-volume method. The soil strength was checked by a hand-held vane shear device. At the end of construction of an entire subgrade section, a dynamic cone penetrometer (DCP) and a light-weight deflectometer (LWD) (ASTM E2835 2011) were used to estimate the subgrade CBR profile and the modulus, respectively.

The pressure cells were installed into the subgrade with the top flushing with the subgrade surface. A geosynthetic layer was placed on the subgrade surface if needed. Similar to the subgrade construction, the base course material was mixed with water to 7.1% moisture content for VGB and 14.1% moisture content for RCA, placed and compacted in two lifts (the first lift was 0.15 m thick and the second lift was 0.1 m thick). The density of each lift was controlled by the weight-volume method. The

target density was set at 95% the maximum dry density determined by the standard Proctor compaction tests. After the construction of the base course, DCP and LWD tests were performed to determine the CBR profile and the modulus. Sand cone tests were also conducted in the base course before the plate loading test by following the ASTM standard (ASTM D1556 2016) to ensure the degree of compaction.

DCP test results were used to estimate the CBR values of each test section. The CBR values were determined using the following equation:

$$\text{CBR} = \frac{292}{(\text{DCPI})^{1.12}} \qquad \text{Eq. 3.1}$$

where DCPI = Penetration Index (mm/blow) (Webster 1993).

Three or four DCP tests were conducted in each test section. Each DCP test was conducted in a quadrant of the test box to ensure the consistency of the test section. Figures 3.14–3.16 show the DCP profiles of all VGB test sections. Figures 3.17–3.19 show the DCP profiles of all RCA test sections.

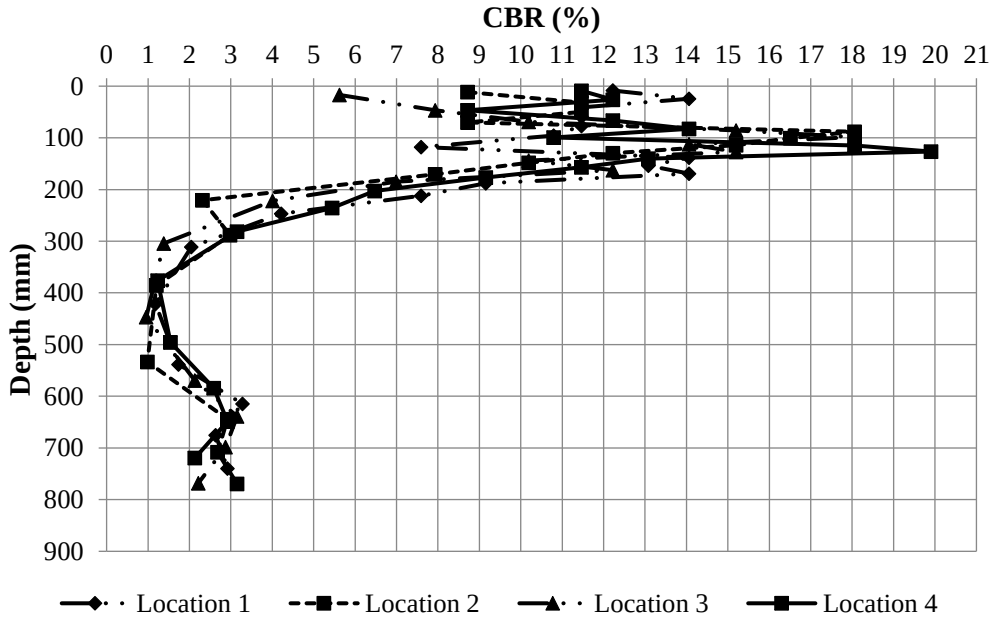

Figure 3.14 CBR profiles for the control VGB test section

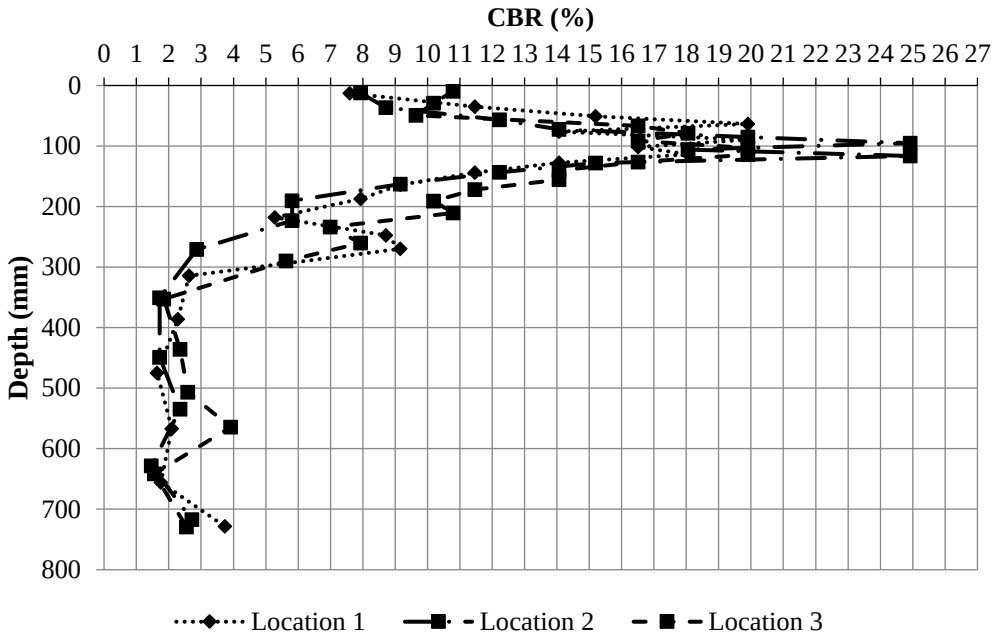

Figure 3.15 CBR profiles for the non-woven geotextile-stabilized VGB test section

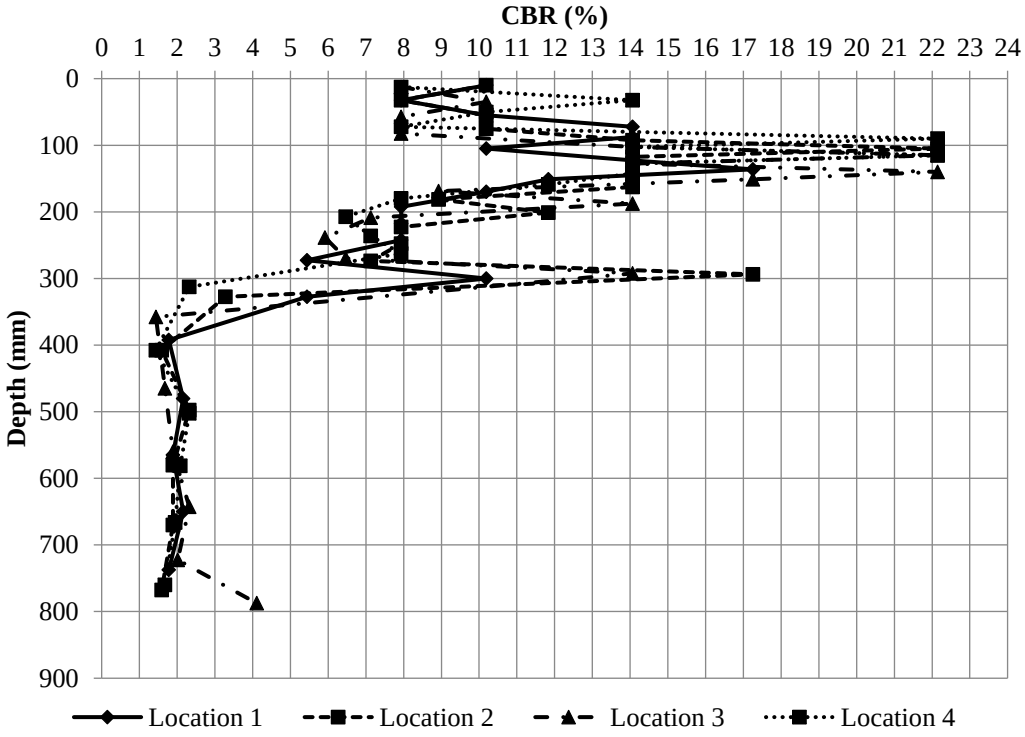

Figure 3.16 CBR profiles for the woven geotextile-stabilized VGB test section

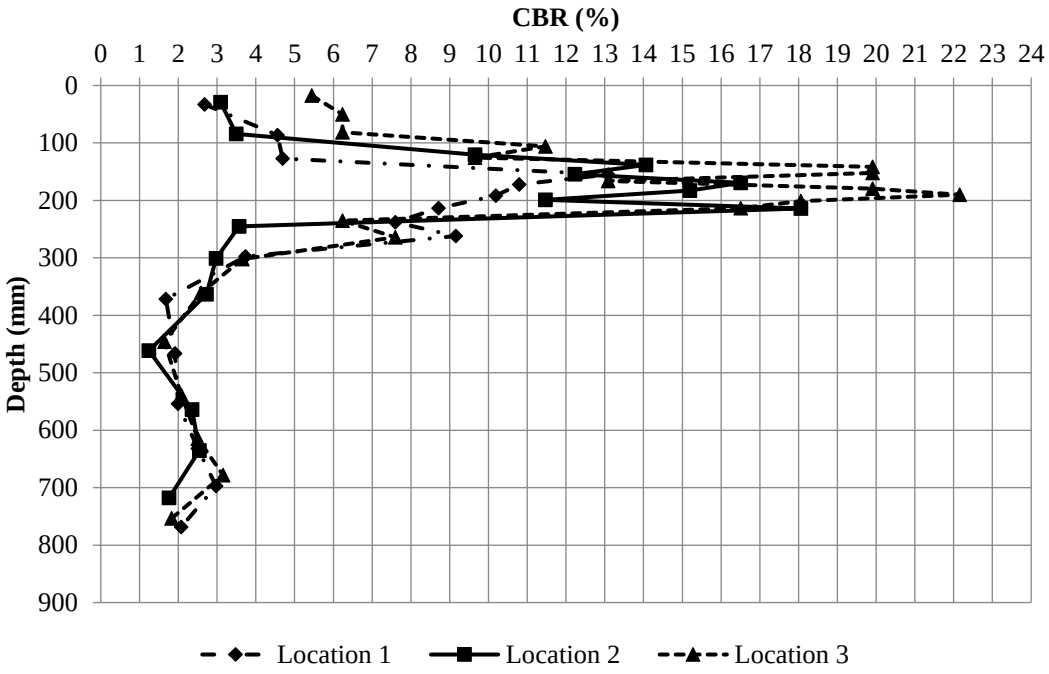

Figure 3.17 CBR profiles for the control RCA test section

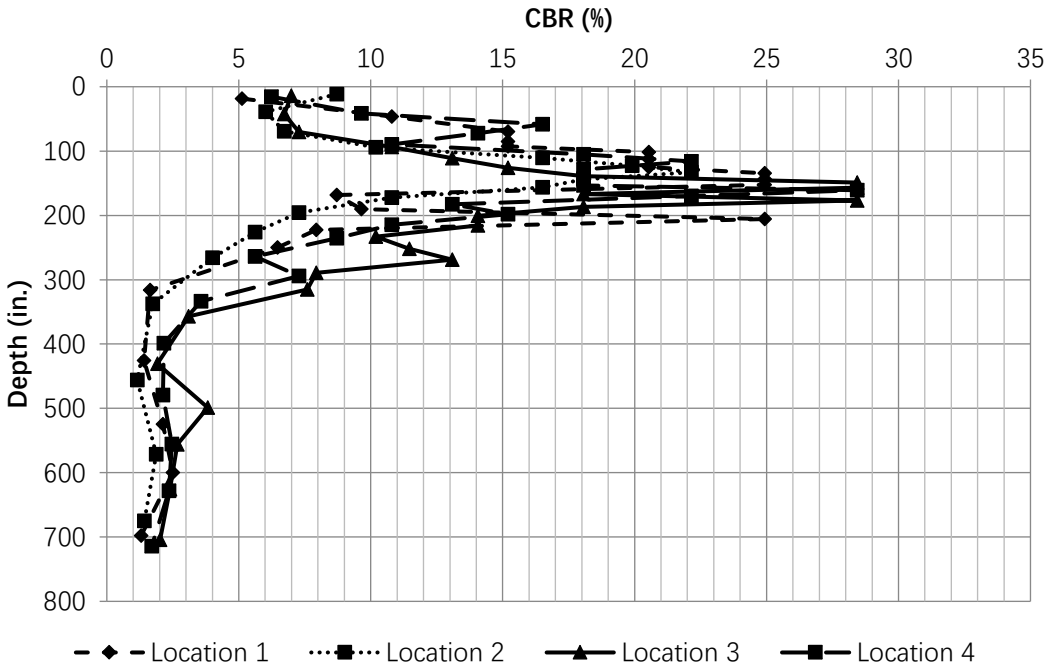

Figure 3.18 CBR profiles for the non-woven geotextile-stabilized RCA test section

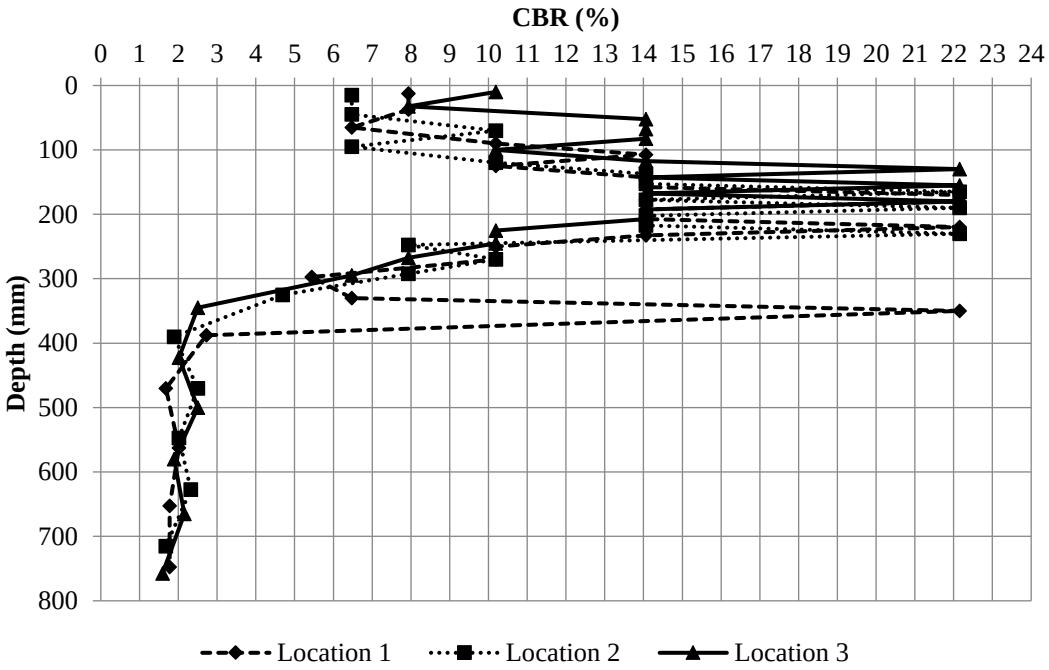

Figure 3.19 CBR profiles for the woven geotextile-stabilized RCA test section

The CBR profiles in the above figures show that in all the test sections, the subgrade CBR was approximately 2% even though there were some variations with depth.

In the base course, the CBR profiles were overall consistent except some spikes, which might result from the penetrometer hitting large aggregate or the geosynthetic layer. The average CBR and coefficient of variation for the subgrade and the base course in each test section are provided in Table 3.2a and b. All values used to calculate the average CBR for base course were taken from depth 0 mm to 250 mm. All values used to calculate the average CBR for subgrade were taken from depth 350 mm to 800 mm. The DCP values at the depths of 250 mm to 350 mm might be affected by the interface where the material either experienced the intermixing or stabilization effect. In stabilized sections, the DCP took extra blows to penetrate the geotextile; therefore, the DCP values at the depths from 250 to 350 mm were not used

to calculate the CBR values.

Table 3.2a Average CBR and coefficient of variation (COV) for subgrade and base course in all VGB sections

VGB	Subgrade CBR		Base Course	
	Average CBR	COV	Average CBR	COV
Control	1.9	0.28	11.5	0.31
NW	2.1	0.30	12.7	0.38
Woven	2.1	0.28	11.9	0.37

Table 3.2b Average CBR and coefficient of variation (COV) for subgrade and base course in all RCA sections

RCA	Subgrade CBR		Base Course	
	Average CBR	COV	Average CBR	COV
Control	2.2	0.23	12.7	0.45
NW	2.1	0.30	15.2	0.43
Woven	2.2	0.48	13.9	0.36

Three to four LWD tests were conducted on the top surface of the subgrade in each test section to ensure the uniformity of the section. Tables 3.3 and 3.4 show the average modulus of each test section. The moduli of the subgrade in different test sections varied but within reasonable ranges. Unfortunately, the LWD measurement for the control RCA section was not taken since the device was not available during that time. The base course stabilized by the woven geotextile had the highest base modulus.

Table 3.3 Subgrade LWD test results

SUBGRADE LWD TEST RESULTS			
VGB Sections	Modulus (MPa)	**RCA Sections**	Modulus (MPa)
Control	4.7	Control	6.5
Non-Woven Geotextile	6.0	Non-Woven Geotextile	6.1
Woven Geotextile	6.6	Woven Geotextile	8.0

Table 3.4 Base course LWD test results

BASE COURSE LWD TEST RESULTS			
VGB Sections	Modulus (MPa)	**RCA Sections**	Modulus (MPa)
Control	14.4	Control	N/A
Non-Woven Geotextile	19.3	Non-Woven Geotextile	14.4
Woven Geotextile	19.7	Woven Geotextile	16.5

After the construction of the base course in each test section, a sand cone test was conducted by following ASTM D1556 / D1556M-15e1 to ensure the dry density of the base course layer to meet the density requirement based on the maximum dry density determined by the standard Proctor compaction tests. Table 3.5 shows the results of the dry density and the degree of compaction for all test sections. The degrees of compaction in all the test sections measured by the sand cone tests were higher than the desired value (95%).

Table 3.5 Sand cone test results for base courses in the test sections

BASE COURSE SAND CONE TEST RESULTS		
	Dry Density (kN/m^3)	Degree of Compaction (%)
VGB Sections		
Control	20.3	95.7
Non-Woven Geotextile	21.0	98.9
Woven Geotextile	22.2	104.8
RCA Sections		
Control	19.1	106.5
Non-Woven Geotextile	17.8	99.1
Woven Geotextile	18.5	103.4

Chapter 4 Results and Analysis

4.1 Introduction

This chapter presents the results of the large cyclic plate loading tests discussed in Chapter 3 and provides the analysis of the test results in terms of total deformation, permanent deformation, elastic deformation, and pressure at the interface between base and subgrade.

4.2 Total Deformation versus Number of Loading Cycles

Each test used incremental loads with a certain number of loading cycles. In the first 1000 cycles, there were five stages that had a small load increment of 13.8 kPa with 200 cycles. Starting from the sixth stage, a large load increment with 2000 cycles was used. The fewer number of load cycles was used for the first five stages because the small load induced a small deformation and the deformation became stable quickly. Due to the small deformation for the first five stages, the geosynthetic was not mobilized and little difference between gesoynthetic-stabilized sections and the control section was observed; therefore, the analysis of test results will focus on the later stages (i.e., the 6^{th} stage and after). Since this research was to evaluate the performance of aggregate bases over weak subgrade for concrete pavement applications, the terminal total deformation was set at 40 mm, which is smaller than 75 mm typically used for unpaved roads.

Figure 4.1 shows the relationship of the measured deformations and the number of cycles for all six test sections. All three RCA test sections finished the entire loading process without reaching the terminal criterion that was set for the total deformation of 40 mm. All VGB test sections reached the terminal criterion before all loading cycles were applied. It is obvious that all RCA sections outperformed the VGB sections.

Figure 4.2 shows the relationship of the deformations and the number of cycles for all VGB test sections. This figure shows that the control section reached the terminal criterion after 9000 cycles, which was at the beginning of the 10th stage of loading and the maximum applied pressure was 345 kPa. The deformation increase rate for the VGB control section was more than the stabilized sections. Also, it took more cycles for the deformation in the control case to become stable. Both stabilized sections performed similarly before the 10th stage. The deformation increase rate became stable at 2000 cycles before the 10th stage. The woven geotextile-stabilized section reached the terminal criterion at the 11,667th cycle (i.e., with the 11th stage and under the applied pressure of 414 kPa) before the non-woven-stabilized section. The woven geotextile-stabilized test section was terminated at the maximum deformation of 39.6 mm. This section reached that deformation. Although the woven geotextile-stabilized section reached the 11th stage, the deformation in the 10th stage did not become stable and showed a trend of increasing deformation. The non-woven geotextile-stabilized section reached the maximum deformation of 39.27 mm at the 12,131th cycle within the 11th stage. In all three VGB sections, the deformations took more cycles to become stable and all sections showed a punching failure mode as shown in Figures 4.4 and 4.5.

Figure 4.3 shows the relationship of the deformation and number of cycles for all three RCA sections. Both stabilized sections behaved similar from the beginning until the end of the 8th stage with the maximum applied pressure of 207 kPa. From the beginning of the 9th stage (276 kPa), the woven geotextile-stabilized section diverged away from the non-woven geotextile-stabilized section. The final maximum deformation for the woven geotextile-stabilized section was 21.44 mm. The maximum deformation for the control section was 21.9 mm. The non-woven geotextile-stabilized section had the least amount of deformation, which had the final maximum deformation of 17.6 mm.

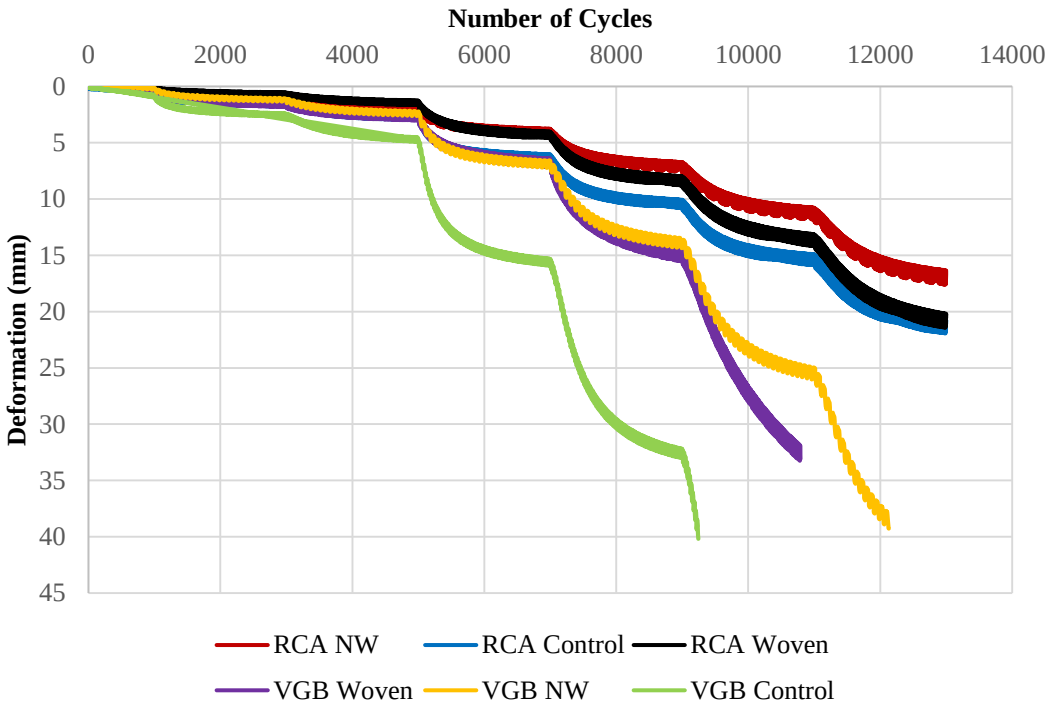

Figure 4.1. Deformation vs. number of cycles for all test sections

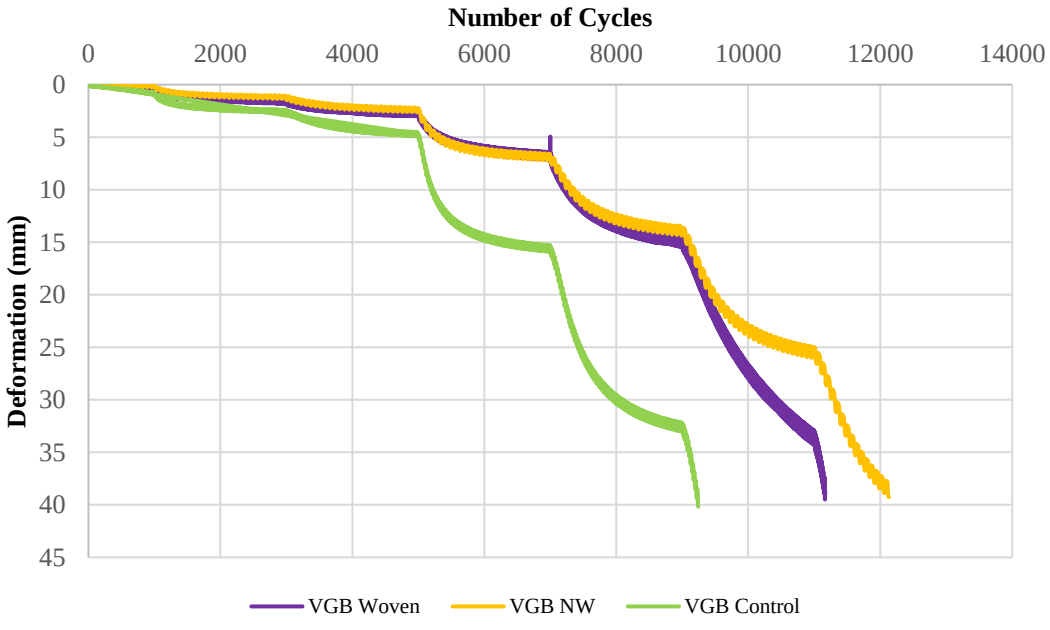

Figure 4.2. Deformation vs. number of cycles for all VGB sections

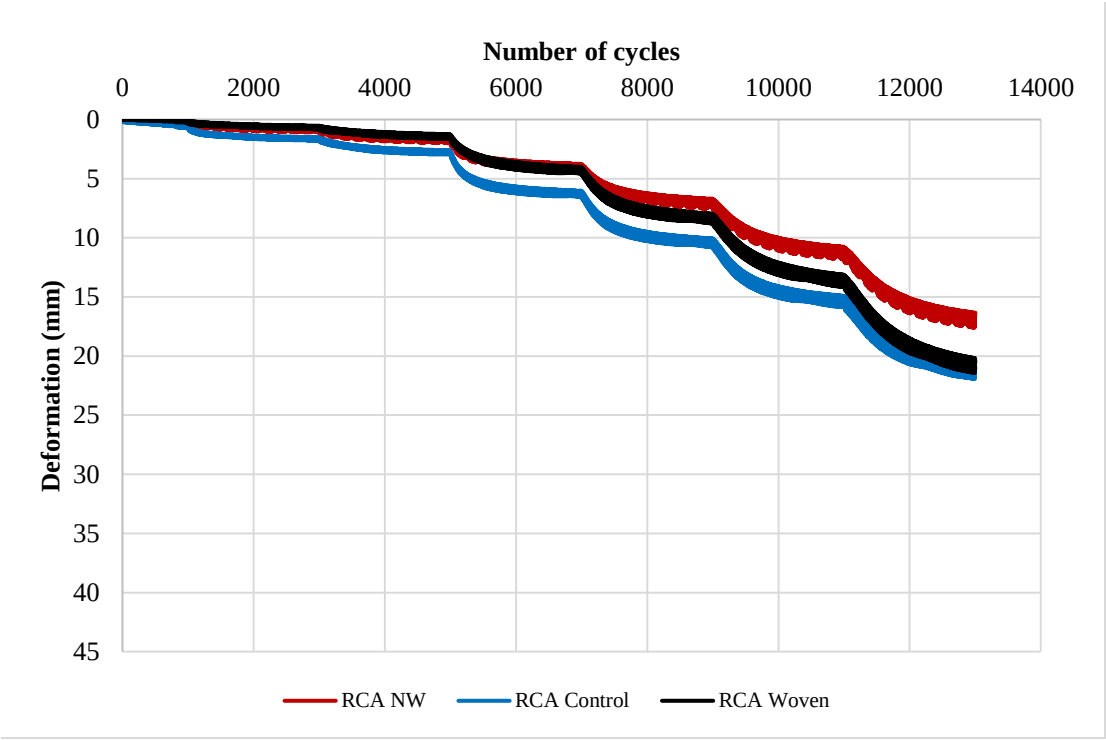

Figure 4.3. Deformation vs. number of cycles for all RCA sections

Figure 4.4 VGB test section showing punching of the loading plate

Figure 4.5 Top view of the VGB test section punched by the loading plate

4.2 Permanent Deformation Result Analysis

Figures 4.1 to 4.3 show the total deformations of the loading plate in all the tests, which include permanent deformation and elastic deformation (or elastic rebound).

This section will discuss the permanent deformation of the test section for each loading stage. Permanent deformations were recorded after unloading to zero pressure for each cycle. Permanent deformations at 0, 200, 400, 600, 800, 1000, 1200, 1400, 1600, 1800, and 2000 cycles were extracted for each loading stage after the 5th stage.

4.2.1 Vertical Permanent Deformation of VGB Sections

Figure 4.6 shows the permanent deformations for all VGB sections in Stage 6 under the applied pressure of 103 kPa. In this stage, the deformation increase rate decreased after 200 cycles and the section deformation became more stable as the number of cycles increased. Table 4.1 shows the permanent deformation for each section at the end of this stage and the accumulated deformation to this stage.

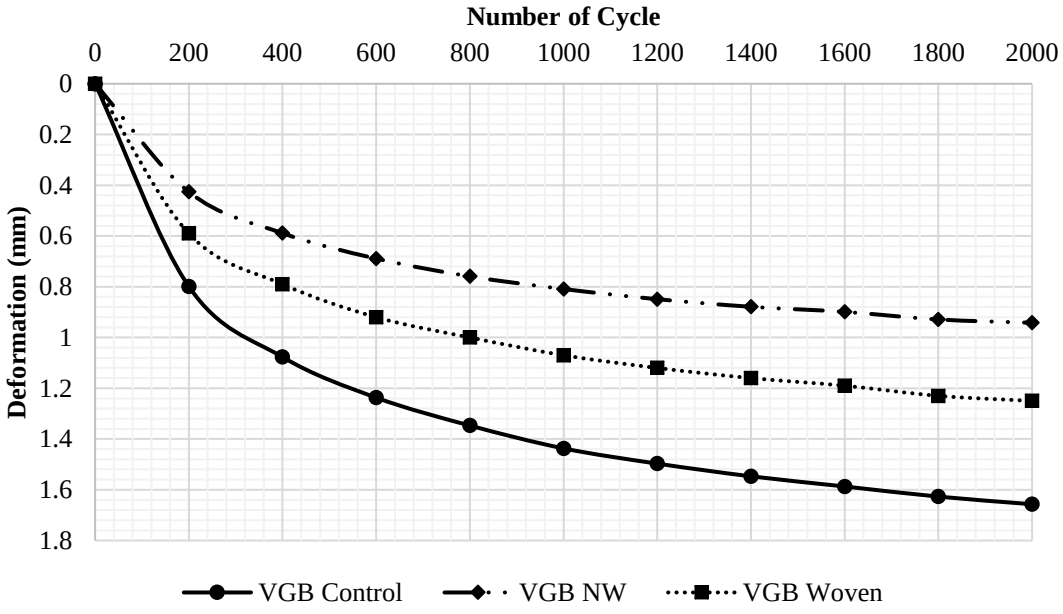

Figure 4.6 Permanent deformation vs. the number of cycles for VGB sections in Stage 6 under the applied pressure of 103 kPa

Table 4.1 Total and Stage 6 permanent deformations for VGB sections

Test section	Total Deformation (mm)	Stage Deformation (mm)
VGB Control	2.39	1.66
VGB NW	1.04	0.94
VGB Woven	1.47	1.25

Figure 4.7 shows the permanent deformations for all VGB sections in Stage 7 under the applied pressure of 138 kPa. In this stage, the two stabilized sections performed almost identically. Due to the increased applied pressure, it took more loading cycles for the deformation to become stable. As shown in the figure, there is no obvious turning point and the deformation increase rate decreased slowly. Table 4.2 shows the permanent deformations for each section at the end of the stage and the accumulated deformation up to this stage.

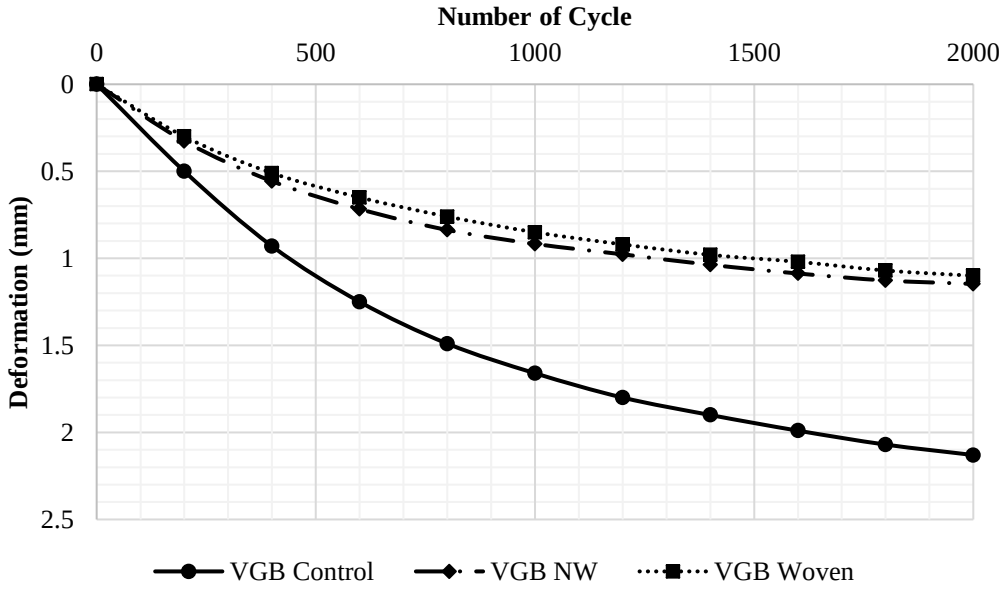

Figure 4.7. Permanent deformation vs. the number of cycles for VGB sections in Stage 7 under the applied pressure of 138 kPa

Table 4.2 Total and Stage 7 permanent deformations for VGB sections

Test Section	Total Deformation (mm)	Stage Deformation (mm)
VGB Control	4.52	2.13
VGB NW	2.19	1.15
VGB Woven	2.57	1.10

In Stage 8, the applied pressure was 207 kPa. In this stage, the two stabilized sections behaved in a similar way as shown in Figure 4.8. The control section had the largest amount of deformation. As shown in Table 4.3, the woven geotextile-stabilized section deformed 3.84 mm in this cycle. The control section had a permanent deformation of 10.78 mm, which is more than the total accumulated deformation up to the previous stage.

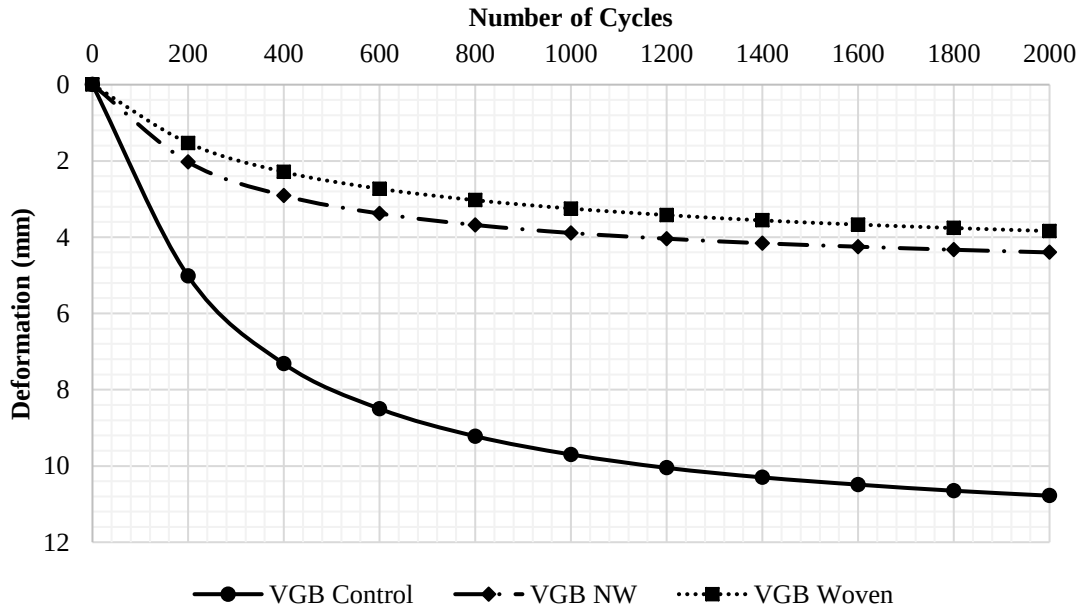

Figure 4.8 Permanent deformation vs. the number of cycles for VGB sections in Stage 8 under the applied pressure of 207 kPa

Table 4.3 Total and Stage 8 permanent deformations for VGB sections

	Total Deformation (mm)	Stage Deformation (mm)
VGB Control	15.3	10.78
VGB NW	6.59	4.4
VGB Woven	6.41	3.84

In Stage 9, the applied pressure was increased to 276 kPa. Figure 4.9 shows that the non-woven geotextile-stabilized section had the best stabilization effect with the least amount of permanent deformation in this stage. The permanent deformation of the control section kept increasing at a large rate. Table 4.4 shows the results of the permanent deformations at the end of this stage.

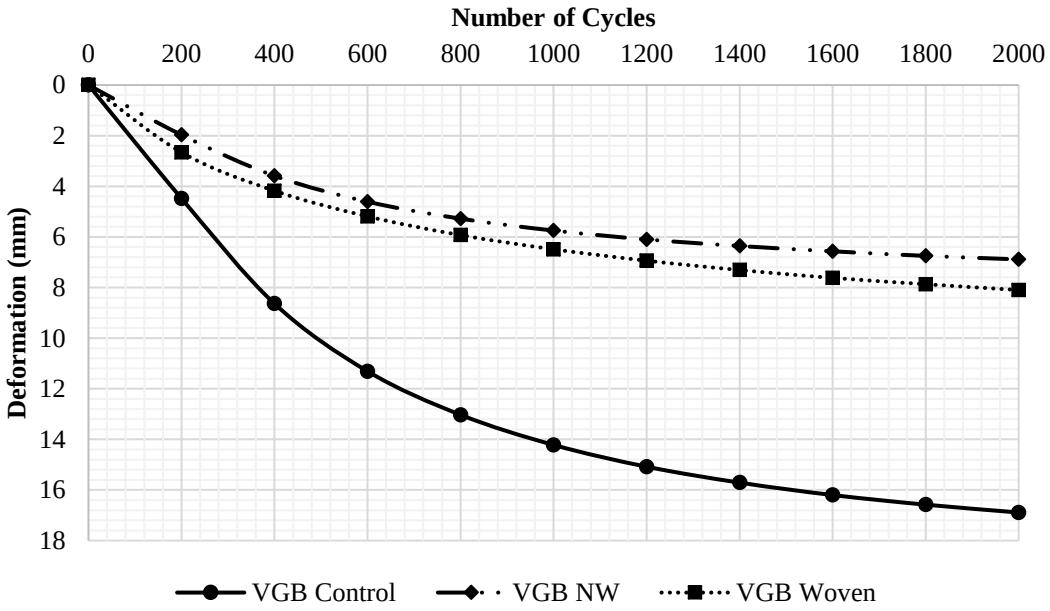

Figure 4.9 Permanent deformation vs. the number of cycles for VGB sections in Stage 9 under the applied pressure of 276 kPa

Table 4.4 Total and Stage 9 permanent deformations for VGB sections

Test Section	Total Deformation (mm)	Stage Deformation (mm)
VGB Control	32.19	16.89
VGB NW	13.48	6.89
VGB Woven	14.51	8.1

In Stage 10, the applied pressure was increased to 414 kPa. The permanent deformation of the control section is not shown in Figure 4.10 since the maximum deformation of this section reached the terminal criterion. In this stage, punching of the loading plate occurred to all sections. Figure 4.10 shows that the deformation curve for the woven geotextile-stabilized section increased at a large rate without showing any stabilization within 2000 cycles. However, the non-woven geotextile-stabilized section had less deformation and increased at a reduced rate with the number of cycles. Table 4.5 shows the results of the stage permanent deformation and the accumulated permanent deformation up to this stage.

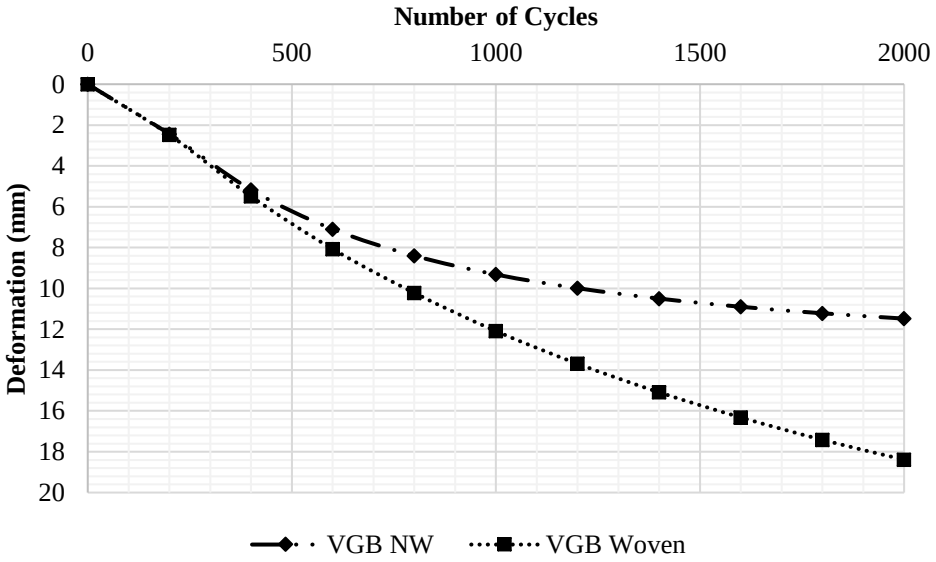

Figure 4.10. Permanent deformation vs. the number of cycles for VGB sections in Stage 10 under the applied pressure of 345 kPa

Table 4.5 Total and Stage 10 permanent deformations for VGB sections

Test Section	Total Deformation. (mm)	Stage Deformation. (mm)
VGB Control	N/A	N/A
VGB NW	24.96	11.48
VGB Woven	32.9	18.39

Table 4.6 shows the total number of loading cycles to the terminal criterion and the total accumulated permanent deformations for all three VGB sections.

Table 4.6 Final permanent deformations and total loading cycles for all VGB sections

Test Section	Total Permanent Deformation. (mm)	Total Cycles
VGB Control	39.09	9243
VGB NW	37.94	12131
VGB Woven	37.8	11666

4.2.2 Vertical Permanent Deformations of RCA Sections

Figure 4.11 shows the performance of all RCA sections in Stage 6. All RCA sections had small deformations. The woven geotextile-stabilized section performed the best and the control section had the largest deformation. Since the applied pressure was relatively low in this stage, the differences among different test sections in this stage might be due to the variations from the construction. Table 4.7 shows the summary of the permanent deformations in all RCA sections in this stage and the total accumulated permanent deformations up to this stage.

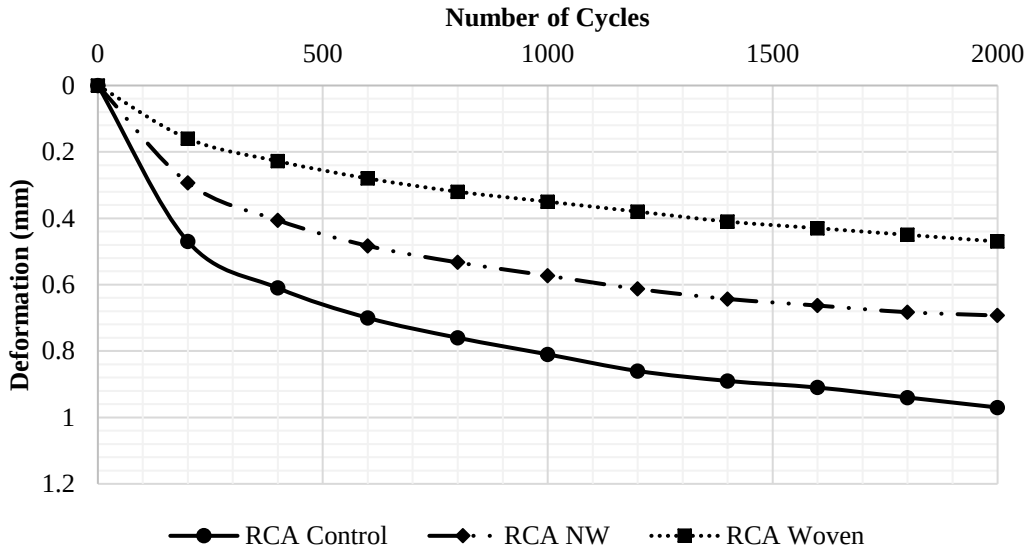

Figure 4.11 Permanent deformation vs. the number of cycles for RCA sections in Stage 6 under the applied pressure of 103 kPa

Table 4.7 Total and Stage 6 permanent deformations for RCA sections

Test Section	Total Deformation. (mm)	Stage Deformation. (mm)
RCA Control	1.52	0.97
RCA NW	0.8	0.693
RCA Woven	0.54	0.47

Figure 4.12 shows the permanent deformation versus number of loading cycles for the RCA sections in Stage 7. It is shown that the stage permanent deformation slightly exceeded that in the previous stage. The woven geotextile-stabilized section had the smallest permanent deformation while the control section deformed the most. All the curves approached to the steady state. Table 4.8 shows the summary of the permanent deformations in all RCA sections for this stage and the total accumulated permanent deformations up to this stage.

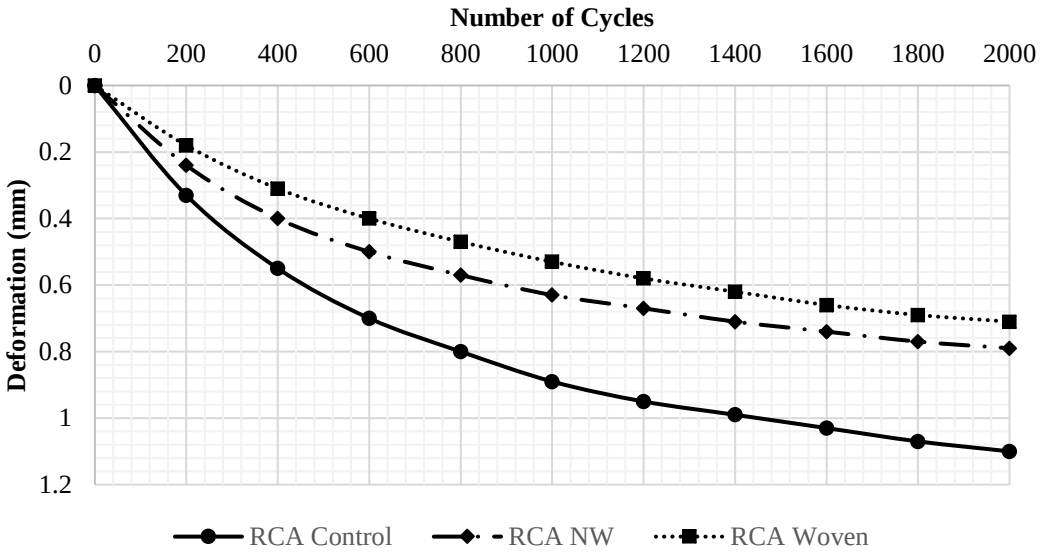

Figure 4.12 Permanent deformation vs. the number of cycles for RCA sections in Stage 7 under the applied pressure of 138 kPa

Table 4.8 Total and Stage 7 permanent deformations for RCA sections

Test Section	Total Deformation. (mm)	Stage Deformation. (mm)
RCA Control	2.62	1.1
RCA NW	1.59	0.79
RCA Woven	1.25	0.71

In Stage 8, the permanent deformations for different RCA sections are shown in Figure 4.13. In this stage, the largest permanent deformations happened in the control section. The non-woven geotextile-stabilized section had the least amount of permanent deformation. All the sections in this stage had stable permanent deformations as the number of cycles increased. No sign of punching failure in any section in this stage was observed. Table 4.9 shows the results of the permanent deformations in this stage and the total accumulated permanent deformations up to this stage.

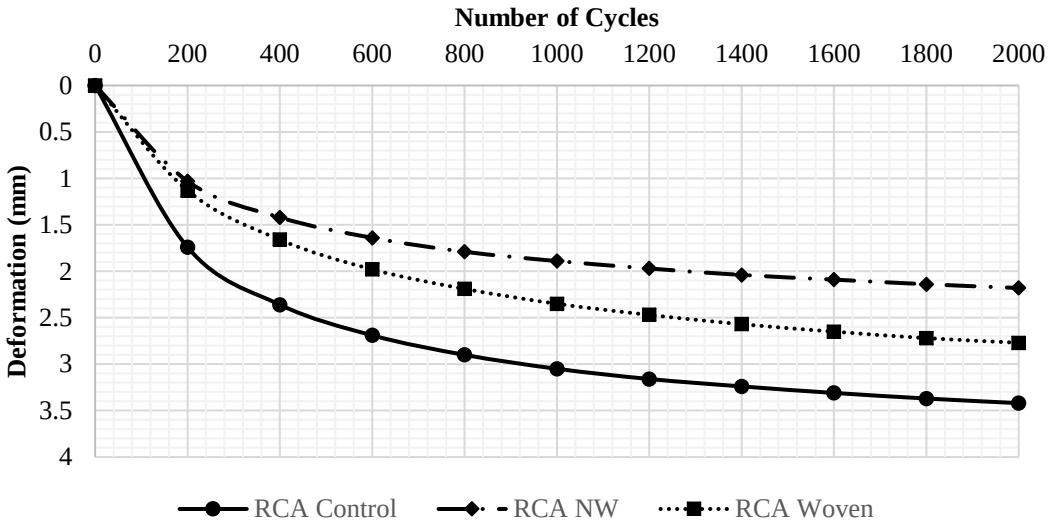

Figure 4.13 Permanent deformation vs. the number of cycles for RCA sections in Stage 8 under the applied pressure of 207 kPa

Table 4.9 Total and Stage 8 permanent deformations for RCA sections

Test Section	Total Deformation (mm)	Stage Deformation (mm)
RCA Control	6.04	3.42
RCA NW	3.77	2.18
RCA Woven	4.02	2.77

Figure 4.14 shows that the permanent deformations versus number of cycles for the RCA sections in Stage 9. The control section and the woven geotextile-stabilized section showed almost identical deformations from 1000 cycles to the end of the stage. The non-woven geotextile-stabilized section had the least permanent deformation. Table 4.10 shows the results of the permanent deformations in this stage and the total accumulated permanent deformations up to this stage.

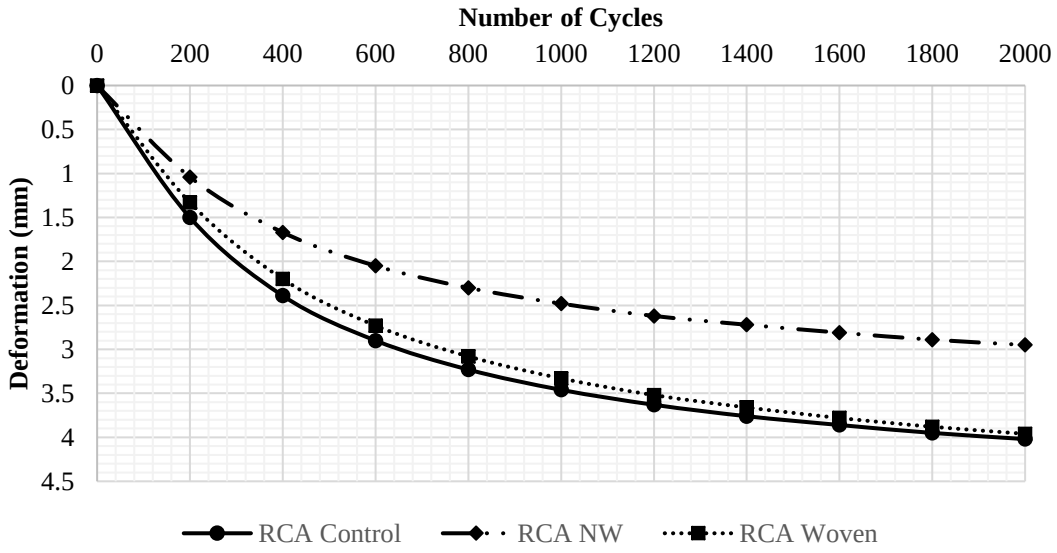

Figure 4.14 Permanent deformation vs. the number of cycles for RCA sections in Stage 9 under the applied pressure of 276 kPa

Table 4.10 Total and Stage 9 permanent deformations for RCA sections

Test Section	Total Deformation (mm)	Stage Deformation (mm)
RCA Control	10.06	4.02
RCA NW	6.72	2.95
RCA Woven	7.98	3.96

Figure 4.15 shows the permanent deformations versus number of cycles for the RCA sections in Stage 10. The increase rates of the permanent deformations in all sections decreased with the number of cycles. The woven geotextile-stabilized section gained the most permanent deformation in this stage and had a steeper curve from the beginning to the end of the stage than other sections. The non-woven geotextile-stabilized section had the least deformations. Table 4.11 shows the total accumulated and stage permanent deformations at the end of this stage.

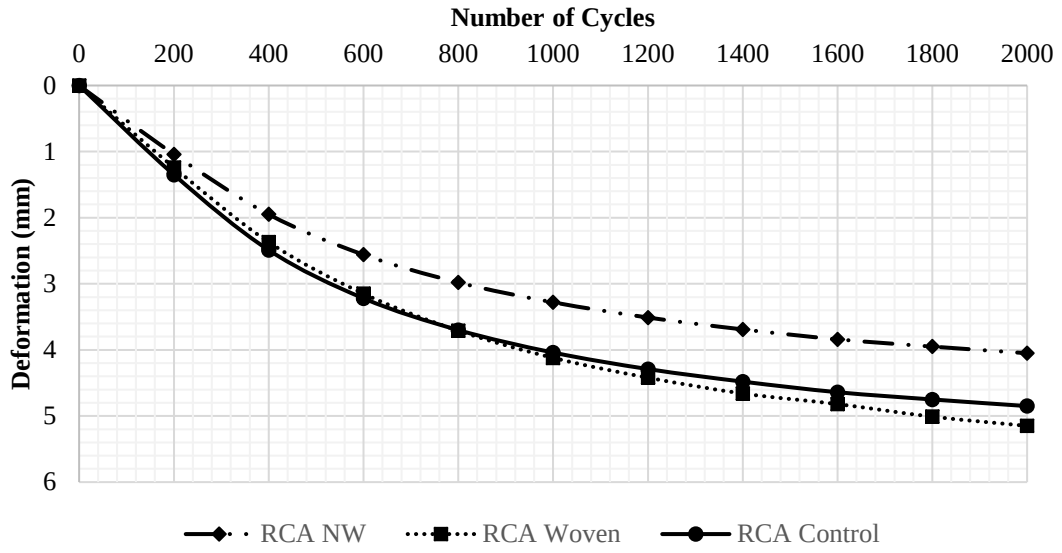

Figure 4.15 Permanent deformation vs. the number of cycles for RCA sections in Stage 10 under the applied pressure of 345 kPa

Table 4.11 Total and Stage 10 permanent deformations for RCA sections

Test Section	Total Deformation (mm)	Stage Deformation (mm)
RCA Control	14.91	4.85
RCA NW	10.77	4.05
RCA Woven	13.13	5.15

In the last stage, the applied pressure was increased to 414 kPa. Under this high pressure, all sections experienced more permanent deformations as shown in Figure 4.16. The woven geotextile-stabilized section had more permanent deformations than the control section and the non-woven geotextile-stabilized section as the number of cycles increased. Table 4.12 shows the results of the final accumulated permanent deformation and the stage permanent deformation.

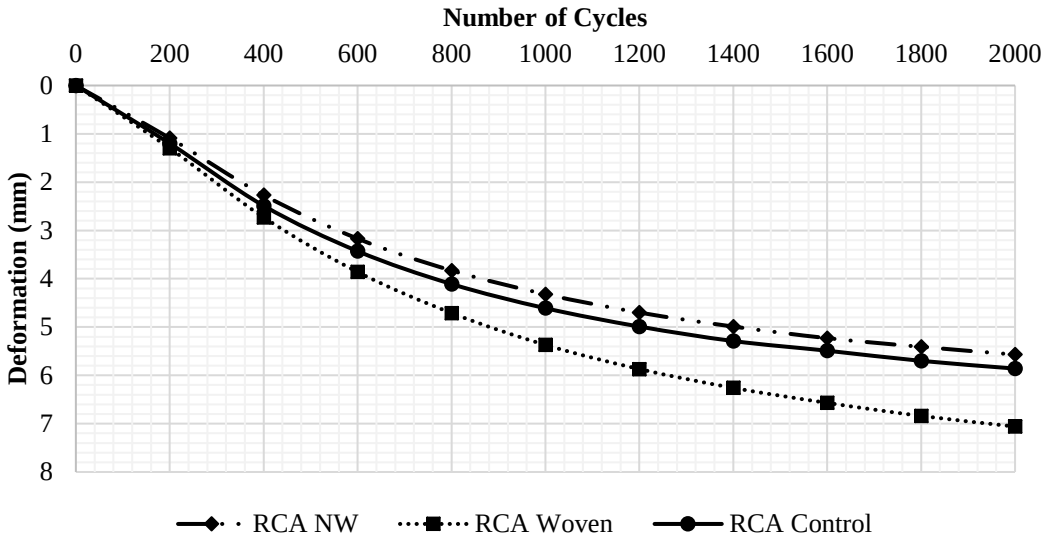

Figure 4.16 Permanent deformation vs. the number of cycles for RCA sections in Stage 11 under the applied pressure of 414 kPa

Table 4.12 Total and Stage 11 permanent deformations for RCA sections

Test Section	Total Deformation. (mm)	Stage Deformation. (mm)
RCA Control	20.77	5.86
RCA NW	16.34	5.57
RCA Woven	20.19	7.06

4.3 Elastic Deformation Analysis

This section will analyze the elastic deformations of all test sections. Elastic deformations are calculated by subtracting the permanent deformation recorded at the end of each stage of loading from the maximum deformation recorded at the end of each stage of loading. Tables 4.13 and 4.14 show the elastic deformations for the VGB sections and the RCA sections, respectively, at the end of each stage for all sections. Both tables show that the elastic deformation increased with the applied pressure. The control section had slightly smaller elastic deformation than both

stabilized sections. The relationship between applied pressure and elastic deformation for both sections are shown in Figure 4.17 and Figure 4.18. The elastic deformation increased almost linearly with the increasing applied pressure. This finding is in agreement with what Sun et al. (2015) concluded. The explanation for this finding offered by Sun et al. (2015) is that the lateral restraint and the tensioned membrane in the stabilized section forced the base material rebound more than in the control section. The RCA sections had smaller larger elastic deformations than the VGB sections because the RCA sections were stiffer than the VGB sections. When the VGB was used, the woven geotextile induced more elastic deformation than the non-woven geotextile because the woven geotextile had higher stiffness than the non-woven geotextile. When the RCA was used, however, the woven geotextile induced similar elastic deformation as the non-woven geotextile because the overall deformations in these sections were small.

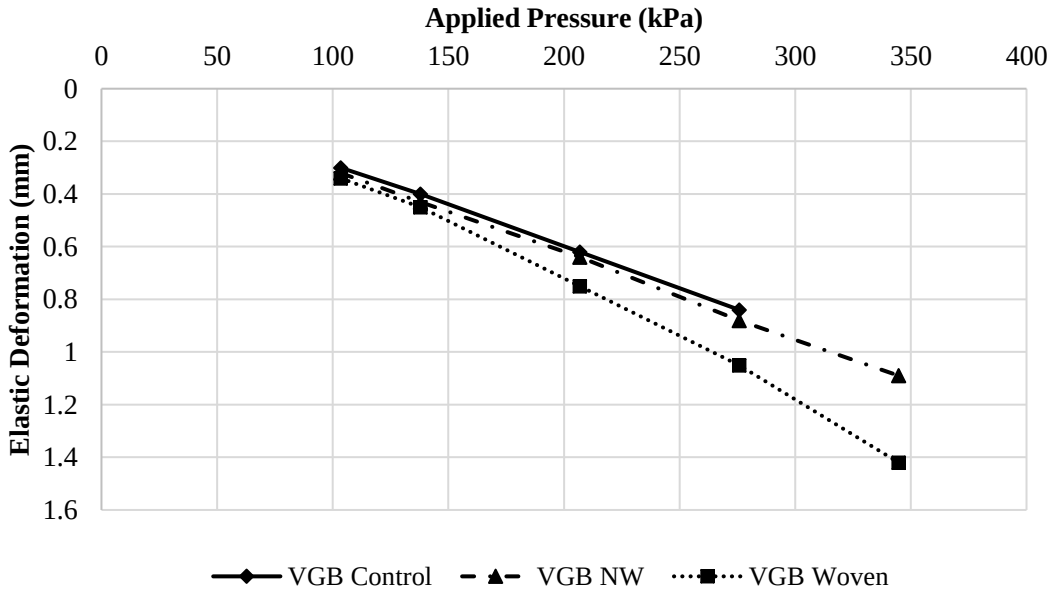

Figure 4.17 Applied pressure vs. elastic deformation for all VGB sections

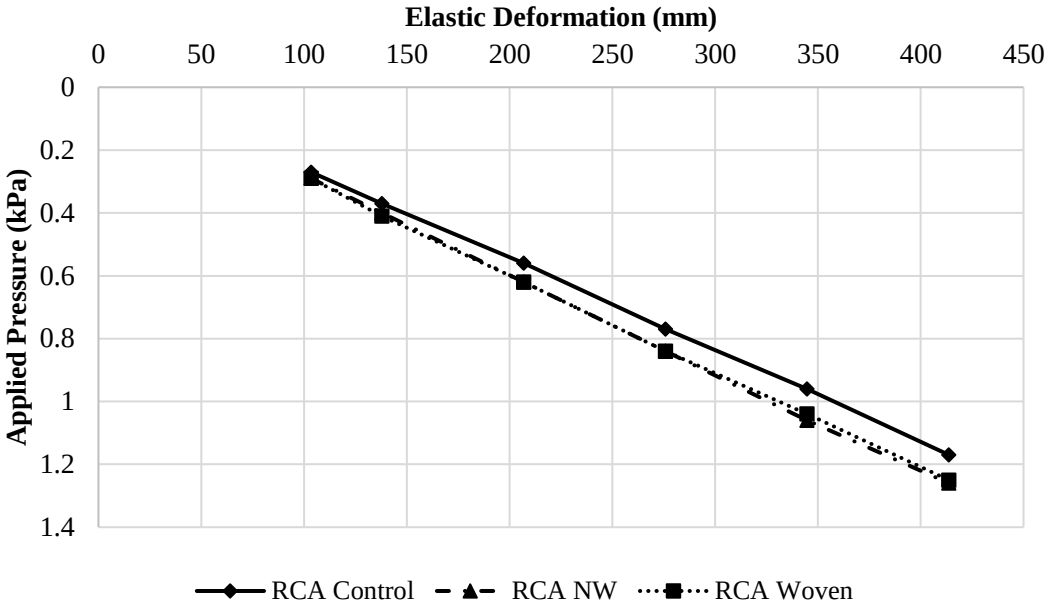

Figure 4.18 Applied pressure vs. Elastic deformation for all RCA sections

Table 4.13 Elastic deformations for all VGB test sections

Stage Number	Applied pressure (kPa)	VGB Control (mm)	VGB NW (mm)	VGB Woven (mm)
6	103.4	0.30	0.32	0.34
7	137.9	0.40	0.43	0.45
8	206.8	0.62	0.64	0.75
9	275.8	0.84	0.88	1.05
10	344.7		1.09	1.42

Table 4.14 Elastic deformations for all RCA test sections

Stage Number	Applied Pressure (kPa)	RCA Control (mm)	RCA NW (mm)	RCA Woven (mm)
6	103.4	0.27	0.29	0.29
7	137.9	0.37	0.4	0.41
8	206.8	0.56	0.62	0.62
9	275.8	0.77	0.84	0.84
10	344.7	0.96	1.06	1.04
11	413.7	1.17	1.26	1.25

4.4 Subgrade Pressure Analysis

Earth pressure cells were installed on top of the subgrade layer to monitor and record the pressures distributed onto the subgrade. Four pressure cells were placed into the subgrade as shown in Figure 3.11 in Chapter 3. The farthest pressure cell did not measure any pressure in all cases and the pressure readings kept fluctuating around 0 kPa; therefore, the data for this earth pressure are not included in the following analysis. The pressure cell at the center (i.e., 0r, r is the radius of the plate) measured the stress distributed directly under the loading plate. The pressure cell located 150 mm (1r) away from the center measured the stress distributed at the edge of the loading plate and the pressure cell at 300 mm (2r) away from the center measured the stress distributed out the loading plate.

In some stages, the pressure cell readings fluctuated above and below 0 kPa; however, the general trend of the vertical pressure distribution on the subgrade was well captured. To minimize this unwanted effect, the net pressure (the highest pressure

recorded towards the end of each stage minus the lowest pressure in the same cycle) was used to represent the pressure at that location in each test section. In the woven geotextile-stabilized VGB section, the data collection frequency was mistakenly set to 1 Hz instead of 10 Hz for all other sections. Since each cycle lasted 1.3 seconds and the logging frequency of 1 Hz was one data/second, some data, such as the peak value of each cycle, might be missed.

Figure 4.19 shows the measured subgrade pressure distributions in all test sections under the applied pressure of 103 kPa in Stage 6. The measured pressures in all the sections show similar distributions. The maximum pressure was located at the center of each test section. All the VGB sections had higher pressures on the subgrade at the center than the RCA sections. This difference can be explained as the VGB had a lower modulus than the RCA. In the VGB sections, the geotextile did not show any benefit in reducing the maximum pressure in the center; however, in the RCA sections, the geotextile did show some benefit.

Figure 4.20 shows the measured subgrade pressure distributions in all test sections under the applied pressure of 138 kPa in Stage 7. In all the RCA sections, the control section recorded the highest subgrade pressure at the center and the lowest subgrade pressure at 2r. The woven geotextile-stabilized section recorded the highest subgrade pressure at the center stress and the lowest stress at 2r. The non-woven geotextile-stabilized section had more uniform subgrade distribution. The VGB sections show the similar effect on the measured subgrade pressure distribution by the geotextiles. All the measured pressures at the center in the VGB sections were higher than those in the RCA sections. In general, the non-woven geotextile-stabilized section experienced the lowest subgrade pressure at the center, followed by the woven geotextile-stabilized section, and the control section.

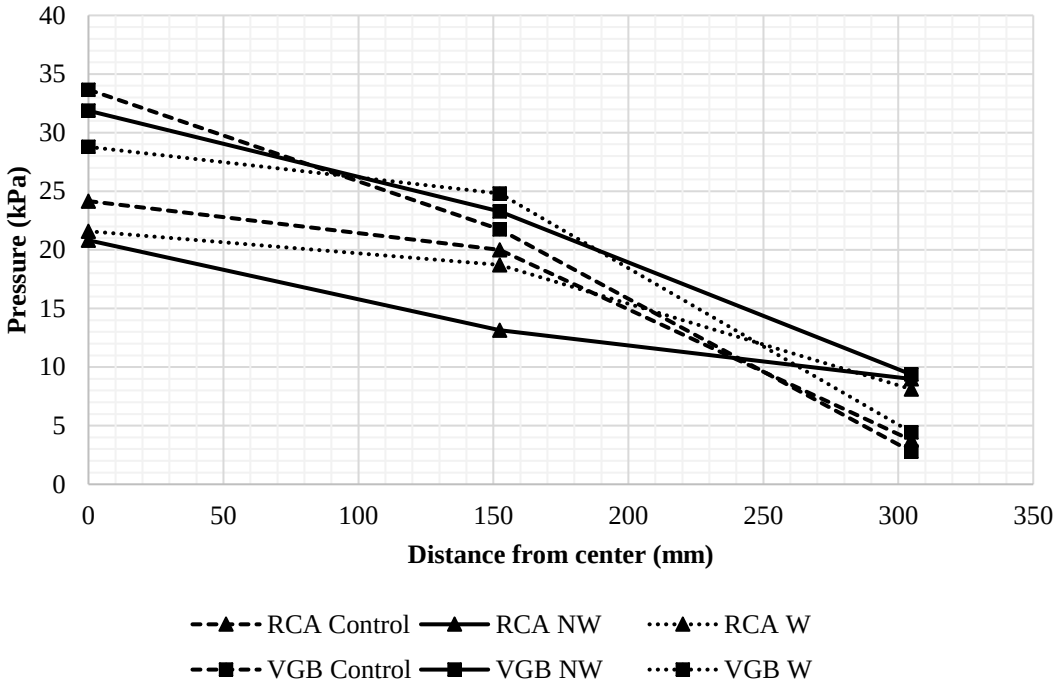

Figure 4.19 Measured subgrade pressures at 0r, 1r, and 2r from the center at the end of Stage 6 loading

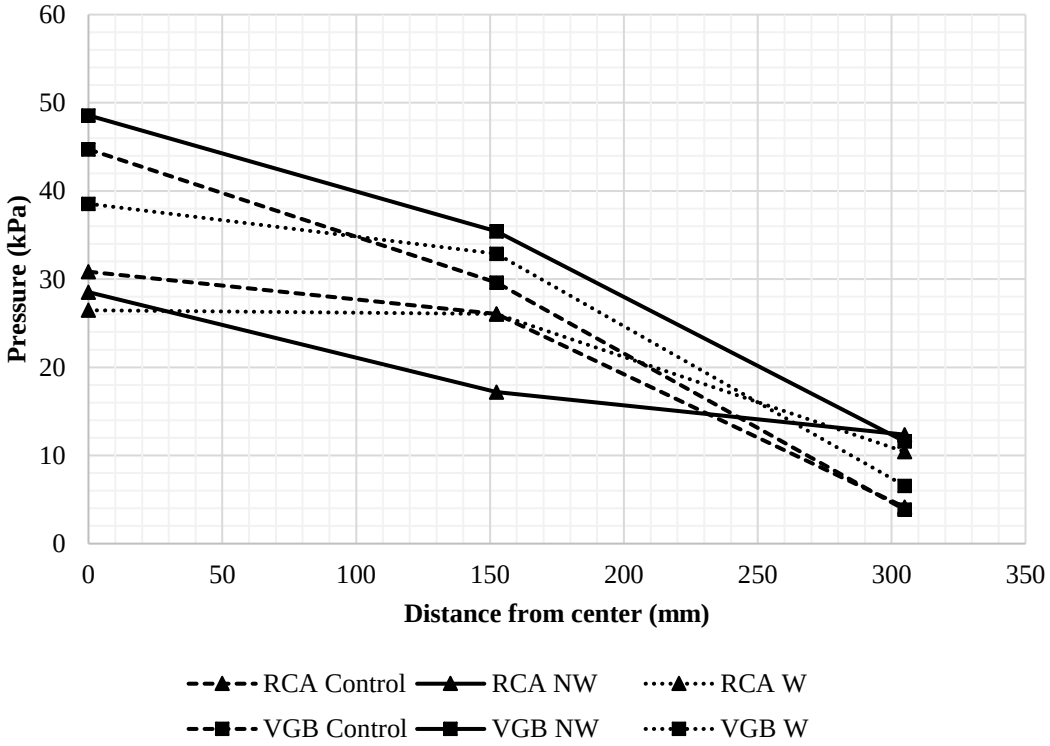

Figure 4.20 Measured subgrade pressures at 0r, 1r, and 2r from the center at the end of Stage 7 loading

Figure 4.21 shows the measured subgrade pressure distributions in all test sections under the applied pressure of 207 kPa in Stage 8. In the RCA sections, the benefit of the stronger geosynthetic reinforcement started to display. The woven geotextile-stabilized section experienced the lowest subgrade pressure at the center. At the same time, the woven geotextile-stabilized section recorded the highest subgrade pressures at 1r and 2r. These results mean the subgrade pressures distributed more uniformly and widely. The non-woven geotextile-stabilized section showed similar behavior except that the subgrade pressure recorded at 1r was 12 kPa lower. The woven geotextile-stabilized VGB section and the non-woven geotextile-stabilized section performed similarly but the non-woven geotextile-stabilized section measured the lower subgrade pressures at all locations.

Figure 4.22 shows the measured subgrade pressure distributions in all test sections under the applied pressure of 276 kPa in Stage 9. In this stage, punching of the loading plate into the VGB sections had an obvious effect on the measured subgrade pressures. Due to punching of the loading plate, the deformation increased drastically, and the pressures were distributed more directly onto the center and the edge of the plate. The woven geotextile-stabilized section had the lowest subgrade pressure at the center but the pressure at 1r was higher than the pressure at the center. The non-woven geotextile-stabilized section showed the similar behavior as the woven geotextile-stabilized section but had higher subgrade pressures. The control section had lower pressures at the farther distance from the center. In the RCA sections, the subgrade pressure at the center in the non-woven geotextile-stabilized section was slightly lower than that in the the control section, but the non-woven geotextile-stabilized section showed a more uniform distribution since the subgrade pressures at 1r and 2 were higher. The woven geotextile-stabilized section outperformed the other

two sections. The measured pressure at the edge in the woven geotextile-stabilized section exceeded the pressure at the center.

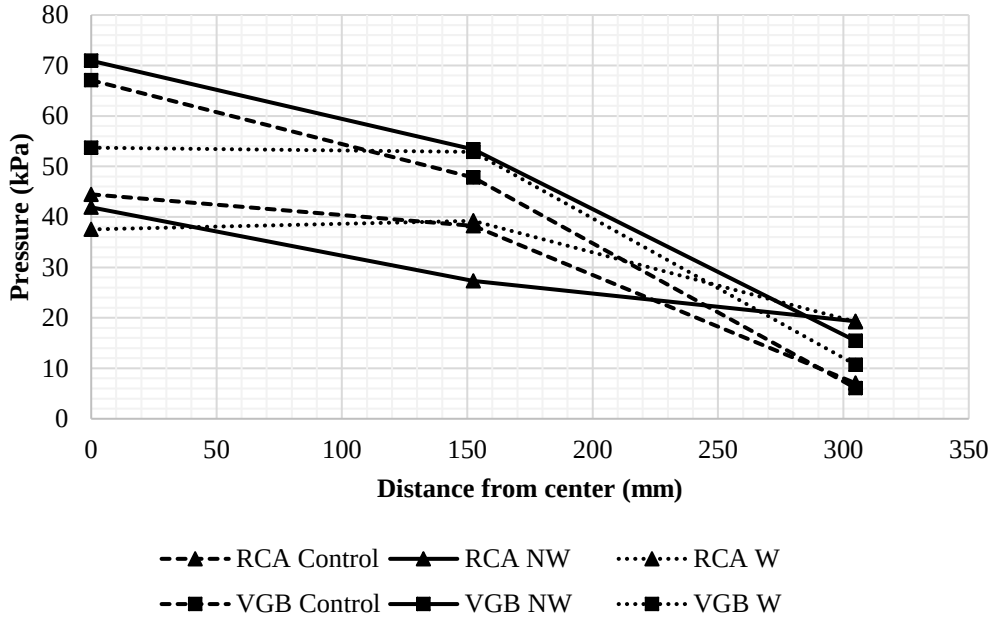

Figure 4.21 Measured subgrade pressures at 0R, 1R, and 2R from the center at the end of Stage 8 loading

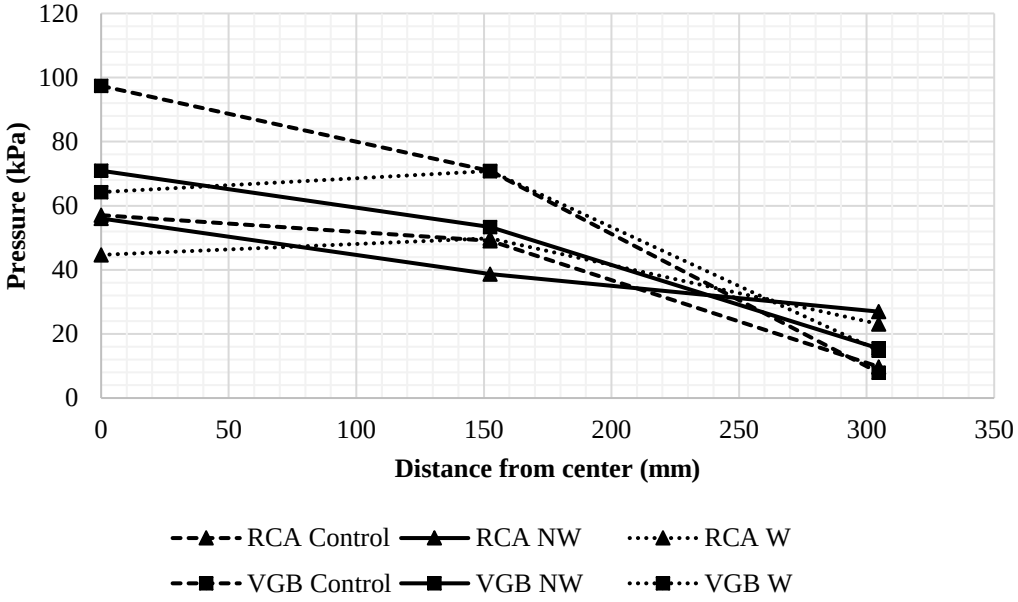

Figure 4.22 Measured subgrade pressures at 0R, 1R, and 2R from the center at the end of Stage 9 loading

Figures 4.23 and 24 show the measured subgrade pressure distributions in all test sections under the applied pressures of 345 kPa in Stage 10 and 413 kPa in Stage 11, respectively. The performances of all the RCA sections were similar to those in the previous stage except that all the measured pressures were higher due to the increased applied pressure. In these two stages, it is obvious that the stronger woven geotextile provided a better stress distribution.

In Stage 10, the non-woven geotextile-stabilized VGB section recorded 99 kPa at the center. The woven geotextile-stabilized VGB section recorded similar pressure at the center and under the edge of the loading plate.

In Stage 11, the measured subgrade pressures at 0r and 1r in the woven geotextile-stabilized VGB section were similar. The non-woven geotextile-stabilized section had higher pressures at all the pressure cell locations.

Tables 4.15 and 4.16 summarize all the measured subgrade pressures in all the test sections from Stages 6 to 11.

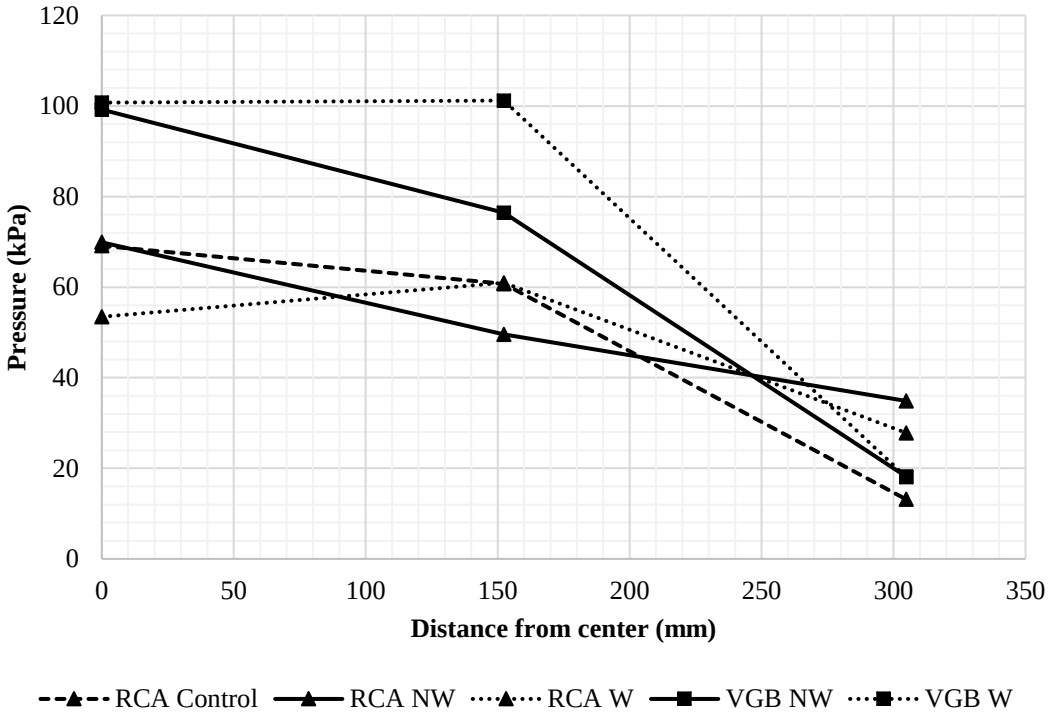

Figure 4.23 Measured subgrade pressures at 0r, 1r, and 2r from the center at the end of Stage 10 loading

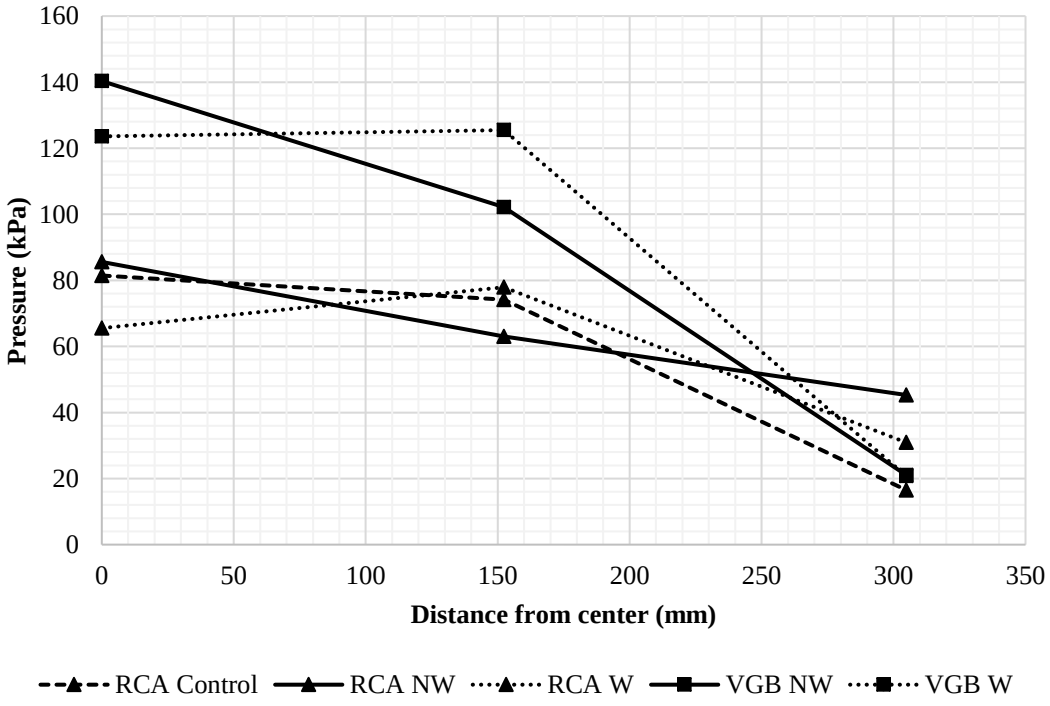

Figure 4.24 Measured subgrade pressures at 0r, 1r, and 2r from the center at the end of Stage 11 loading

At the end of Stage 11, the woven geotextile-stabilized section had lower subgrade pressure at the center and higher pressures at farther distances. The reason the woven geotextile could distribute the load more uniformly is because of the tensioned membrane effect.

Table 4.15 Measured subgrade pressures in all RCA sections at 0R, 1R, and 2R at the end of stage loading

	Location	RCA CONTROL	RCA NW	RCA Woven	RCA GG
Stage 6	0r (kPa)	24	21	22	24
	1r (kPa)	20	13	19	9
	2r (kPa)	4	9	8	6
Stage 7	0r (kPa)	31	29	26	29
	1r (kPa)	26	17	26	11
	2r (kPa)	4	12	10	9
Stage 8	0r (kPa)	44	42	38	40
	1r (kPa)	38	27	39	14
	2r (kPa)	7	19	19	11
Stage 9	0r (kPa)	57	56	45	47
	1r (kPa)	49	39	50	24
	2r (kPa)	10	27	23	16
Stage 10	0r (kPa)	69	70	53	61
	1r (kPa)	61	50	61	36
	2r (kPa)	13	35	28	21
Stage 11	0r (kPa)	81	86	66	76
	1r (kPa)	74	63	78	53
	2r (kPa)	17	45	31	23

Table 4.16 Measured subgrade pressures in all VGB sections at 0R, 1R , and 2R at the end of stage loading

	Location	VGB Control	VGB NW	VGB Woven	VGB GG
6	0r (kPa)	34	25	29	28
	1r (kPa)	22	19	25	11
	2r (kPa)	3	7	4	2
7	0r (kPa)	45	32	39	40
	1r (kPa)	30	23	33	15
	2r (kPa)	4	9	7	3
8	0r (kPa)	67	49	54	58
	1r (kPa)	48	35	53	23
	2r (kPa)	6	12	11	3
9	0r (kPa)	97	71	64	79
	1r (kPa)	71	53	71	33
	2r (kPa)	8	15	15	3
10	0r (kPa)		99	101	99
	1r (kPa)		76	101	48
	2r (kPa)		18	18	3
11	0r (kPa)		140	124	119
	1r (kPa)		102	125	65
	2r (kPa)		23	21	3

4.5 Comparison of Base Material Performance

Under the same loading sequence, the total accumulated permanent deformation in the VGB control section at 9000 cycles was 31.5 mm. However, the total accumulated permanent deformation at 9000 cycles in the RCA control section was 9.5 mm. The VGB control section was not able to have stable deformations within 2000 cycles starting from Stage 9 and its deformation curve indicated possible bearing failure. At the end of Stage 9, however, the permanent deformation of the RCA control section was stabilized. Figure 4.25 shows that the RCA control section outperformed the VGB control section in terms of permanent deformations.

In terms of the measured subgrade pressures, the RCA sections could distribute the load better than the VGB sections. For example, the applied pressure in Stage 9 was 276 kPa. The measured maximum subgrade pressure in the RCA control section was 57 kPa at the center, 49 kPa at 1R, and 10 kPa at 2R. Under the same applied pressure, the subgrade pressure in the VGB control section was 97 kPa at the center, 71 kPa at 1R, and 8 kPa at 2R. This comparison means that the load was more concentrated under the loading plate in the VGB sections than in the RCA sections.

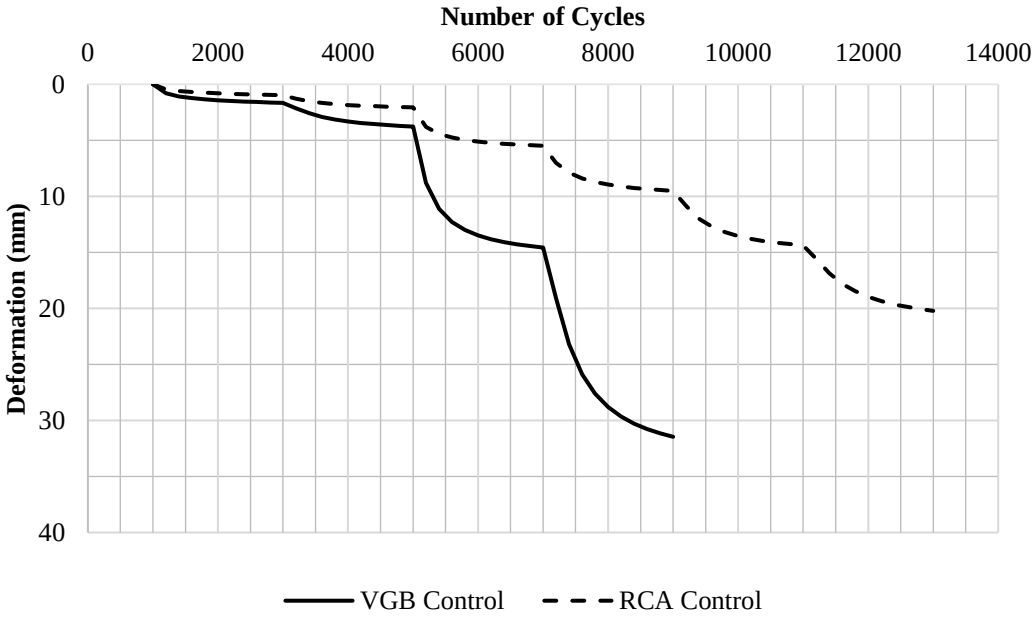

Figure 4.25 Permanent deformations in the VGB and RCA control sections

Chapter 5 Conclusions and Recommendations

5.1 Conclusions

This study was performed to evaluate the performance of recycled concrete aggregate (RCA) versus virgin granular base (VGB) used with non-woven and woven geotextiles. Six large-scale cyclic plate loading tests were performed. Total deformations (elastic and permanent deformations) and subgrade pressures were monitored during different stages of loading. Below are the conclusions from this study:

1. The performance of the RCA base course in terms of permanent deformation and load distribution was superior to that of the VGB, which is commonly used by the Kansas Department of Transportation (KDOT).

2. Non-woven geotextile and woven geotextile reduced the permanent deformations of the base course over weak subgrade as compared with the control sections. Based on the geosynthetic products selected in this study, the non-woven geotextile performed better than the woven geotextile because it could have better interaction with aggregates than the woven geotextile.

3. Non-woven geotextile and woven geotextile reduced the maximum subgrade pressures and helped distribute the load to a wider area and more uniformly. The benefit of the woven geotextile became more obvious at large deformations due to the tensioned membrane effect.

4. The non-woven geotextile and woven geotextile-stabilized sections had slightly larger elastic deformations than the control sections because the inclusion of the geotextile induced more elastic rebound by lateral restraint and tensioned membrane.

5.2 Recommendations for Future Studies

1. All the experimental tests were conducted inside the geotechnical testing box at the University of Kansas. A small hand-held vibrating plate compactor was used to compact the base courses. The compaction energy generated by the compactor was lower than that by a full-scale vibrating roller. The density, modulus, and strength of the base course might affect the test results. The above conclusions should be verified by field tests.

2. Geosynthetic products used in the study were selected from the KDOT geosynthetic product approval list. Their material properties are not similar; therefore, it should be caution to make direct comparisons of their performance.

3. All the test sections in this study were subjected to limited load magnitudes and cycles during a short time period. RCA may degrade in a long term and degradation of RCA may affect its performance. This effect should be investigated in the future.

4. This study only investigated the performance of the base courses over weak subgrade with a fixed California Bearing Ratio of approximately 2%. The effect of subgrade modulus and strength on the performance should be further investigated.

References

American Association of State Highway and Transportation Officials (AASHTO) (1993). *Guide for design of pavement structures*. Washington, D.C.

American Association of State Highway and Transportation Officials (AASHTO) (2011). *Standard specifications for transportation materials and methods of sampling and testing*. Washington, D.C.

American Association of State Highway and Transportation Officials (AASHTO) (2015). *Standard Specification for Reclaimed Concrete Aggregate for Unbound Soil—Aggregate Base Course*. Washington, D.C.

American Association of State Highway and Transportation Officials (AASHTO) (2015). *Mechanistic-Empirical Pavement Design Guide: A Manual of Practice.* Washington, D.C.

American Association of State Highway and Transportation Officials (AASHTO). (1999). "Determining the resilient modulus of soils and aggregate materials." *T-307-99, TS-1a*. Washington, D.C.

Arulrajah, A., Piratheepan, J., Disfani, M. M., and Bo, M. W. (2012). "Geotechnical and geoenvironmental properties of recycled construction and demolition materials in pavement subbase applications." *Journal of Materials in Civil Engineering,* 25(8), 1077-1088.

Abbot Jr., David M. 2017. "The mineral baby; Iconic graphic continues to tell important story." *Mining Engineering* (Society for Mining, Metallurgy, & Exploration) 69 (6): 41-45.

ASTM D1140. (2017). *"Standard Test Methods for Determining the Amount of Material Finer than 75-mu-m (No. 200) Sieve in Soils by Washing."* West Conshohocken, PA: American Society for Testing and Materials (ASTM) International.

ASTM D1556. (2016). "*Standard Test Method for Density and Unit Weight of Soil in Place by Sand-Cone Method."* West Conshohocken, PA: American Society for Testing and Materials (ASTM) International.

ASTM D1883. (2016). *" Standard Test Method for California Bearing Ratio (CBR) of Laboratory-Compacted Soils."* West Conshohocken, PA: American Society for Testing and Materials (ASTM) International.

ASTM D2166. (2016). *" Standard Test Method for Unconfined Compressive Strength of Cohesive Soil."* West Conshohocken, PA: American Society for Materials and Testing (ASTM) International.

ASTM D2573. (2015). "*Standard Test Method for Field Vane Shear Test in Saturated Fine-Grained Soils."* West Conshohocken, PA: American Society for Testing and Materials (ASTM) International.

ASTM D421. (2007). *" Standard Practice for Dry Preparation of Soil Samples for Particle-Size Analysis and Determination of Soil Constants."* West Conshohocken, PA: American Society for Testing and Materials (ASTM) International.

ASTM D4318. (2010). *"Standard Test Methods for Liquid Limit, Plastic Limit, and Plasticity Index of Soils."* West Conshohocken, PA: American Society for Materials and Testing (ASTM) International.

ASTM D4643. (2017). "*Standard Test Method for Determination of Water Content of Soil and Rock by Microwave Oven Heating."* West Conshohocken, PA: American Society for Testing and Materials (ASTM) International.

ASTM. (2018). *"Standard Test Method for Use of the Dynamic Cone Penetrometer in Shallow Pavement Applications."* West Conshohocken, PA: American Society for Testing and Materials (ASTM) International).

ASTM D698. (2012). *" Standard Test Methods for Laboratory Compaction Characteristics of Soil Using Standard Effort (12,400 ft-lbf/ft3 (600 kN-m/m3))."* West Conshohocken, PA: American Society for Testing and Materials (ASTM) International.

Bennert, T., Papp Jr, W., Maher, A., and Gucunski, N. (2000). "Utilization of construction and demolition debris under traffic-type loading in base and subbase applications." *Transportation Research Record: Journal of the Transportation Research Board*(1714), 33-39.

Black, P., and Holtz, R. (1999). "Performance of geotextile separators five years after installation." *Journal of geotechnical and geoenvironmental engineering*, 125(5), 404-412.

Chesner, W. H, Collins R.J, and MacKay M.H (1998). "User guidelines for waste and by-product materials in pavement construction." *Report No. FHWA-RD-97-148*. U.S. Dept. of Transportation, Washington, D.C.

Chidiroglou, I., Goodwin, A., Laycock, L., and O'Flaherty, F. (2008). "Physical properties of demolition waste material." *Proceedings of the Institution of Civil Engineering Journal Construction Materials*(CM3), 97-103.

Dong, Y.-L., Han, J., and Bai, X.H. (2010). "Bearing capacities of geogrid-reinforced sand bases under static loading." *Ground Improvement and Geosynthetics*, 275-281.

Garber, S., and Rasmussen, R. (2010). "Nonwoven geotextile interlayers in concrete pavements." *Transportation Research Record: Journal of the Transportation Research Board*(2152), 11-15.

Giroud, J., and Han, J. (2004). "Design method for geogrid-reinforced unpaved roads. II. Calibration and applications." *Journal of Geotechnical and Geoenvironmental Engineering*, 130(8), 787-797.

Giroud, J. P., and Han, J. (2004). “Design method for geogrid-reinforced unpaved roads-Part I: Theoretical development.” *Journal of Geotechnical and Geoenvironmental Engineering*, 130(8), 775-786.

Giroud, J. P., and Han, J. (2004). "Design method for geogrid-reinforced unpaved roads. I. Development of design method." *J. Geotech. Geoenviron. Eng.*, 130(8), 775-786.

Gonzalez, G., and Moo-Young, H. (2004). "Transportation applications of recycled concrete aggregate." *FHWA state of the Practice National Review*.

Han, J. (2015). "Principles and practice of ground improvement." Hoboken, New Jersey : John Wiley & Sons, Inc.

Hein, D. K., Rao, S., and Lee, H. (2016). "Bases and Subbases for Concrete Pavements." *FHWA-HIF-16-005. 2016,* U.S. Dept. of Transportation, Washington, D.C.

Hufenus, R., Rueegger, R., Banjac, R., Mayor, P., Springman, S. M., and Brönnimann, R. (2006). "Full-scale field tests on geosynthetic reinforced

unpaved roads on soft subgrade." *Geotextiles and Geomembranes*, 24(1), 21-37

KDOT. 2018. *STANDARD SPECIFICATIONS FOR STATE ROAD & BRIDGE C ONSTRUCTION*. May 28.

Kermani, B., Xiao, M., Stoffels, S. M., and Qiu, T. (2018). "Reduction of subgrade fines migration into subbase of flexible pavement using geotextile." *Geotextiles and Geomembranes*, 46(4), 377-383.

Maxwell, S., Kim, W., Edil, T. B., and Benson, C. H. (2005). "Effectiveness of geosynthetics in stabilizing soft subgrades." *Report to the Wisconsin Department of Transportation (2005)*.

Melbouci, B. (2009). "Compaction and shearing behaviour study of recycled aggregates." *Construction and Building Materials*, 23(8), 2723-2730.

Montanelli, F., Zhao, A., and Rimoldi, P. "Geosynthetic-reinforced pavement system: testing and design." *Proc., Proceeding of Geosynthetics*, 619-632.

Pokharel, S. K., Han, J., Leshchinsky, D., Parsons, R. L., and Halahmi, I. (2010). "Investigation of factors influencing behavior of single geocell-reinforced bases under static loading." *Geotextiles and Geomembranes*, 28(6), 570-578.

Poon, C. S., and Chan, D. (2006). "Feasible use of recycled concrete aggregates and crushed clay brick as unbound road sub-base." *Construction and building materials*, 20(8), 578-585.

Qian, Y., Han, J., Pokharel, S. K., and Parsons, R. L. (2013). "Performance of Triangular Aperture Geogrid-Reinforced Base Courses over Weak Subgrade under Cyclic Loading." *Journal of Materials in Civil Engineering*, 25(8), 1013-1021.

Sivakumar, V., McKinley, J., and Ferguson, D. (2004). "Reuse of construction waste: performance under repeated loading." *Proceedings of the Institution of Civil Engineers-Geotechnical Engineering*, 157(2), 91-96.

Subaida, E., Chandrakaran, S., and Sankar, N. (2009). "Laboratory performance of unpaved roads reinforced with woven coir geotextiles." *Geotextiles and Geomembranes*, 27(3), 204-210.

Sullivan, Daniel E., "Material in Use in U.S. Interstate Highways," *United States Geological Survey Fact Sheet 2006-3127*, October 2006.

Sun, X., Han, J., and Corey, R. (2017). "Equivalent modulus of geogrid-stabilized granular base back-calculated using permanent deformation." *Journal of Geotechnical and Geoenvironmental Engineering*, 143(9), 06017012.

Sun, X., Han, J., Kwon, J., Parsons, R. L., and Wayne, M. H. (2015). "Radial stresses and resilient deformations of geogrid-stabilized unpaved roads under cyclic plate loading tests." *Geotextiles and Geomembranes*, 43(5), 440-449.

Tam, V. W., and Tam, C. M. (2007). "Crushed aggregate production from centralized combined and individual waste sources in Hong Kong." *Construction and Building Materials*, 21(4), 879-886.

Webster, S. L. (1993). "Geogrid reinforced base courses for flexible pavements for light aircraft: literature review and test section design." *Miscellaneous Paper GL-92-6.* U.S. Army Corps of Engineers Waterways Experiment Station, Vicksburg, MS.

White, D. J., and Vennapusa, P. K. (2017). "In situ resilient modulus for geogrid-stabilized aggregate layer: A case study using automated plate load testing." *Transportation Geotechnics*, 11, 120-132.